


Article

Mapping Water Bodies and Wetlands from Multispectral and SAR Data for the Cross-Border River Basins of the Polish–Ukrainian Border

Tetiana Melnychenko and Tatiana Solovey * 

Polish Geological Institute—National Research Institute, 00-975 Warsaw, Poland; tetiana.melnichenko@pigi.gov.pl or meltanua777@gmail.com

* Correspondence: tatiana.solovey@pigi.gov.pl; Tel.: +48-22-459-2149

Abstract: Using remote sensing data to accurately record water surface changes over large areas is crucial in monitoring water resources. However, mapping water surfaces from remote sensing data has its advantages and disadvantages. This study presents a method for mapping water surfaces and wetlands based on Sentinel-1/-2 data over a study area of more than 26,000 km² in three river basins, the Bug, Dniester, and San, located along the Polish–Ukrainian border. To achieve this goal, an image processing algorithm with additional options was developed (special filters, type classification, and post-classification), which minimized the shortcomings and increased the accuracy of the method. As a result, by using optical and radar data, it was possible to create maps of water bodies in the study area in the driest month of the year from 2018 to 2021. The results were evaluated numerically and graphically. The accuracy of the method was assessed using the Kappa coefficient. For optical data, the lowest value was 76.28% and the highest was 88.65%; for radar data, these values were 87.61% and 97.18%, respectively. When assessing accuracy, the highest values were achieved for overall accuracy (OA), with a maximum of 0.95 (for SAR) and 0.91 (for optical data). The highest values were in user accuracy (UA), with a maximum value of 1 for both SAR and optical data.

Keywords: water surface; remote sensing; Sentinel-1/-2; optical data; SAR data; Lee filter; MLC classification; post classification; accuracy coefficient Kappa



Citation: Melnychenko, T.; Solovey, T. Mapping Water Bodies and Wetlands from Multispectral and SAR Data for the Cross-Border River Basins of the Polish–Ukrainian Border. *Water* **2024**, *16*, 407. <https://doi.org/10.3390/w16030407>

Academic Editors: Guido D'Urso, Hao Zhang, Yuanbin Cai and Rui Zhou

Received: 10 November 2023

Revised: 19 January 2024

Accepted: 22 January 2024

Published: 26 January 2024



Copyright: © 2024 by the authors. Licensee MDPI, Basel, Switzerland. This article is an open access article distributed under the terms and conditions of the Creative Commons Attribution (CC BY) license (<https://creativecommons.org/licenses/by/4.0/>).

1. Introduction

In recent years, data from various sources (NASA, NOAA, USGA, and ESA) have recorded climatic and environmental changes that affect the condition and quality of water systems, both on a global and local scale. As humanity is facing the problem of fresh (drinking) water shortages, there is a need to thoroughly research river systems and rapidly record changes in water surfaces over time. The periodic and accurate monitoring of water resources based on the rapid registration of changes in water surfaces is also necessary. An effective method for solving this problem is the use of remote sensing data.

Scientists have successfully applied remote sensing technologies in hydrogeological, environmental, and geological research using optical and radar data from various satellites: Sentinel-1 [1–10]; Sentinel-2 [2,3,7–20]; Landsat-1, -2, and -3–8 [10,12,14,15,21–33]; MODIS (Terra/Aqua) [24,34–43]; ASTER (Advanced Spaceborne Thermal Emission and Reflection Radiometer) [19,24,44]; ASAR (Advanced synthetic Aperture Radar) [1,36,45–48]; AVHRR (Advanced Very High Resolution Radiometer) [36,49]; NOAA (National Oceanic and Atmospheric Administration); LIDAR [21,36,50]; and ENVISAR [36,45,48]. Researchers often use Sentinel-1/2–5 data products, which have been open access on the Copernicus Open Access Hub platform since 2014, as well as Landsat-1/2, 3–8, MODIS (Terra/Aqua), and NOAA, ones also available to consumers.

To map the watercourses and detect hydrological changes, scientists use a set of water (or humidity) indices, like NDWI (Normalized Water Difference Index), MNDWI

(Modified Normalized Difference Water Index), AWEI (Automated Water Selection Index), SWI (SAR Water Index), WRI (Water Ratio Index) and, additionally, NDVI (Normalized Difference Vegetation Index) and NDMI (Normalized Difference Moisture Index) [1–5,7–18,20,29,33,34,42–48,50–52].

Each of the indices has its own formula, but most researchers improve them by adding data from the several bands of satellite sensors or from the satellites themselves, allowing for an increased resolution, the recording of clear changes, and the attainment of better results [1–5,9,10,26–31,33–35,38,39,42–46]. The use of RGB compositions [40,41] helps to identify the areas with the appropriate characteristics (humidity, evaporation, surface water, vegetation, urban development, mountains, fields, etc.) and attain the long-term observation of changes on the surface of seas, rivers, lakes, and wetlands.

The types of satellite data can be divided into two categories: optical data and radar data. The first has a wide spectral range, allowing for the identification of numerous objects, but it is dependent on weather conditions (cloudy days are not observable). The second type enables the finding of objects regardless of weather conditions (cloudiness, fog, etc.), but it has a more complex processing algorithm: geocoding (dereferencing), using the various filters to reduce “noise”, correcting false areas (incorrectly classified areas), etc.

Optical satellite data are used for mineral and lithology mapping. For example, in northeastern Morocco, using combinations of ASTER and Sentinel-2A spectral bands in RGB compositions, scientists identified lithological units and updated the geological mapping at a scale of 1:50,000 [19]. Using Sentinel-2 data, the scientists applied a technique based on the MNDWI and NDWI spectral indices of water [18]. As a result, the monitoring was accurate, which became an important component for mapping water bodies with a 10 m and 20 m resolution.

Regarding the use of only SAR radar data (Sentinel-1) for studying water surfaces, it is important to apply the various filters while processing satellite images to reduce “noise”, increase the clarity of the image of water body borders, and improve the formula of the appropriate index [1,4–7,45,46,52]. Recently (2020–2022), studies using combinations of SAR data (VV and VH polarization) with optical data have become common [2,3,5,6,10], which allows for optimal results to be obtained with respect to studying the dynamics of and changes in the water surface and wetlands.

Generally, to solve the hydrogeological problems of determining the areas of water bodies (rivers, lakes, reservoirs, and shorelines) and obtaining the humidity values, the NDWI, MNDWI, AWEI, and SWI indices are used, the formulae of which are expressed through the satellite bands. For example, the NDWI has a rather simple formula that corresponds to the ratio of the difference of Green to NIR to their sum, where Green is the visible green band (the wavelength is 0.5425–0.5775 nm for Sentinel-2) and NIR is the near-infrared band (the wavelength is 0.7845–0.8995 nm for Sentinel-2). The formula is as follows:

$$\text{NDWI} = (\text{Green} - \text{NIR}) / (\text{Green} + \text{NIR}), \quad (1)$$

Green band waves penetrate clear water quite well, making it possible to notice the contrast between the clear and turbid water band (NIR) and making it well suited for mapping shorelines and biomass content, as well as vegetation detection and analysis.

MNDWI is a modified NDWI index, where SWIR is the shortwave infrared band (for Sentinel-2: 1.36–1.39 and 1.565–1.655 nm); the formula is as follows:

$$\text{MNDWI} = (\text{Green} - \text{SWIR}) / (\text{Green} + \text{SWIR}), \quad (2)$$

The SWIR band is useful for measuring the moisture values in soil and vegetation, and it provides a good contrast between different types of vegetation.

AWEI (Automated Water Extraction Index) is an index that distinguishes snow from clouds and has a more complex formula:

$$\text{AWEI} = 4 \times (\text{Green} - \text{SWIR2}) - (0.25 \times \text{NIR} + 2.75 \times \text{SWIR1}), \quad (3)$$

AWEI is a water selection index that separates the water and non-water pixels in such a way that zero serves as a threshold that can segment the land cover into a binary image of dry land and water.

The SWI (SAR Water Index) is used by researchers [1–7,17,45–47] to identify the water surface regardless of cloudiness and weather conditions. The SWI has a simple formula where only SAR data are applied; when VV and VH have a dual polarization, it is the ratio of VV to VH (Sentinel-1):

$$\text{SWI} = \text{VH}/\text{VV} \text{ or } \text{VH} - \text{VV}/\text{VH} + \text{VV}, \quad (4)$$

Sentinel-1 C-band SAR devices can operate in the single polarization of HH or VV and the dual polarization of HH + HV or VV + VH; they are implemented through one transmission circuit (switchable to H or V) and two parallel reception circuits for H and V polarization (accessed on 1 June 2022, <https://sentinels.copernicus.eu/web/sentinel/user-guides/sentinel-1-sar>). To identify water surfaces, VH and VV polarizations are used separately (without formulas) [1–6] or in an RGB composite (VV, VH, VH/VV [6]; RGB: VV, VH, (VV-VH)) [7].

The ability to penetrate clouds determines the suitability of using SAR data for monitoring changes in water bodies. However, the presence of noise significantly complicates the processing algorithm and requires the use of various filters. Optical data are noise-free but are dependent on weather conditions; monitoring is not possible on cloudy days. Also, optical data have a wide spectral range, which allows for the identification of numerous objects.

It is possible to solve the problem of accurately mapping water bodies using remote data by successfully selecting satellite data, improving the image processing method (adding various options), and using water indices with an improved formula. A methodology for the accurate identification of water surfaces for the study area would help to track temporal changes in water bodies and identify drought/wetting trends that lead to a decrease in drinking water supply and, in the future, track climate change (climate warming). The goal of this study was (1) to develop a method for the accurate identification of water bodies using remote sensing data for the study area and (2) to map and calculate the area of water surfaces and wetlands in the driest month of the year from 2018 to 2021. This study constitutes the first time this has been carried out for three river basins, the Bug, Dniester, and San, located along the Polish–Ukrainian border, using satellite image processing data (optical and radar). Based on the results obtained by scientists [1–8,10,17,20,25,36,45–47,52,53] using radar and optical data with different processing methods (application of filters, classification types, and post-classification), we decided to use Sentinel-1 and Sentinel-2 satellite images in this research and develop the most optimal methodology for identifying water surfaces and drought/wet areas over a large study area with contrasting relief and natural features.

2. Study Area

The study area includes three transboundary river basins on the Polish–Ukrainian border: the Bug, San, and Dniester (Figure 1). The basins lie at the intersection of the Eastern European Plain and the Carpathian region in southeastern Poland and northwestern Ukraine. The three river basins cover a total area of over 26,000 km².

All three river basins are located close to each other, but they should be described separately because each river has individual hydrogeological and geographical characteristics.

The river basin areas have contrasting reliefs (mountains, depressions, and plains) and different “surface coverage” (forests, fields, water bodies, and urbanization); these factors must be included in remote data processing. The Bug basin is the largest in terms of area and is located in the East European Plain. The northern part of the basin, within Western Polissia, is dominated by denudation, accumulative plains with a slight slope, and numerous peat bogs, swamps, and lakes. The southern part is within the Volhynian Upland and, in Ukraine, the Volhynian–Podolsk Upland. The annual precipitation over the

last forty years ranged from 500 mm in Polesie to 600–700 mm in the Volhynian Upland. In the period covered by the analysis, the field evaporation ranged from 450 mm/year to 470 mm/year [54,55].

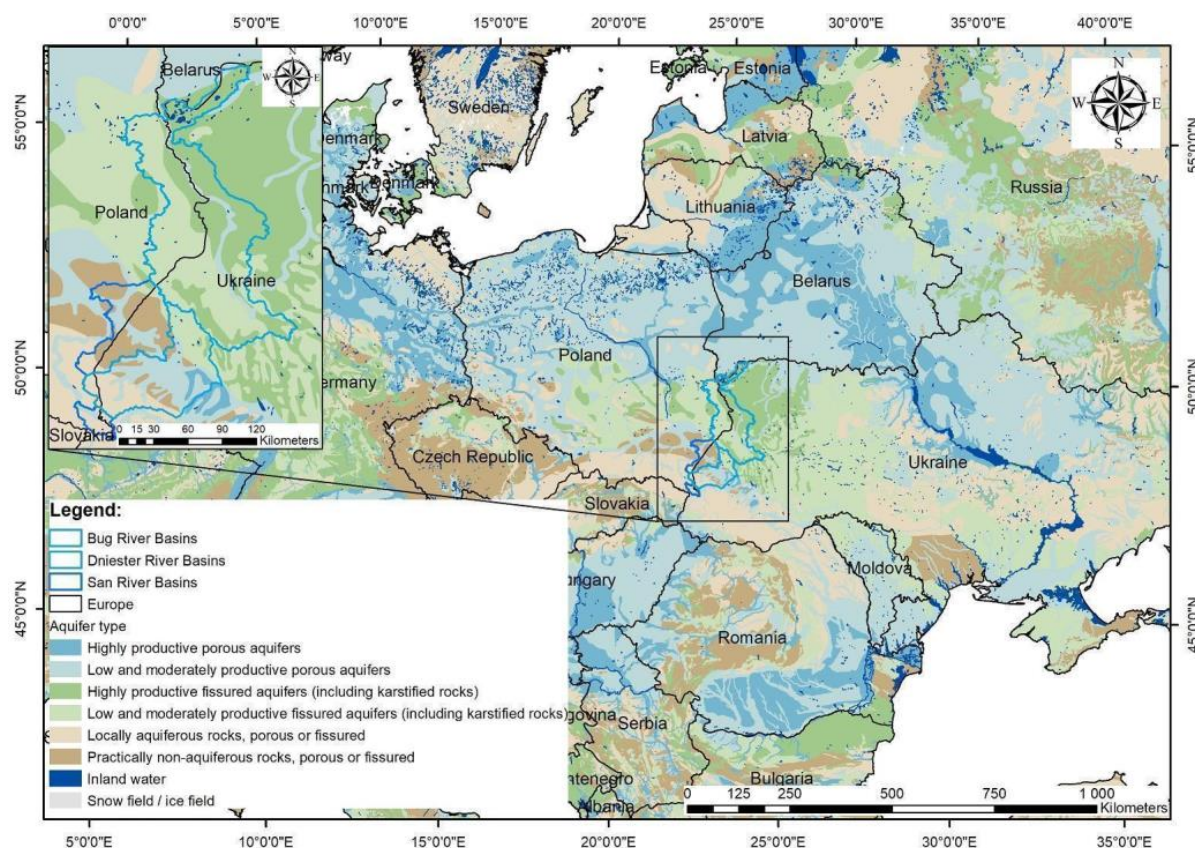


Figure 1. Overview map of the location study area of the basin rivers of the Bug, San, and Dniester (data BRG <https://www.bgr.bund.de>).

The majority of the Dniester River basin is located in Ukraine and belongs to three geological and tectonic units: the northern part is Roztocze, which belongs to the Volhynian–Podolian Upland; the central part is Subcarpathia, which is situated within the Subcarpathian depression; and the southern part, the Eastern Beskids, is connected with the Outer Flysch Carpathians [54].

The territory of the San River basin is located in Roztocze in the northern part, constitutes part of the Carpathian region, and belongs to three geological and tectonic units: Roztocze, the Volhynian–Podolian Upland; part of the Carpathian Foredeep; and the southern part, Eastern Beskids, which is connected to the Outer Flysch Carpathians.

3. Materials and Methods

In order to select the input data and research method, we first familiarized ourselves with the contemporary research in the literature. For example, scientists from Italy have improved image processing technology by enhancing the SWIR band for the MNDWI from Sentinel-2 images [18]. As a result, they obtained MNDWI images with a 10 m spatial resolution and mapped the Venice coastline [18]. The improvement of the accuracy of the methodology’s algorithms by automating water extraction using SAR data, separately or in combination with multispectral Landsat-8 and Sentinel-2 images, was presented by scientists from Brazil [10], resulting in the accurate monitoring of water levels in Brazilian reservoirs [10].

Using the NDWI and Sentinel-2 data, researchers [11] monitored a lake with wetland areas and clarified its hydrological conditions. The authors of [22] developed an algorithm

using the NDWI, NDVI, and simultaneous measurements of water levels in the shallow lake of the Natural Park of Albufera. As a result, the methodology proved to be a useful environmental tool for monitoring the flood cycle of a wetland and was capable of detecting even the lowest water levels [22].

In [20], the authors enhanced the MNDWI image (10 m resolution) by sharpening the Sentinel-2 MSI image based on the NDWI for urban surface water mapping. The results showed that the proposed MNDWI image exhibited a higher resolution and was more effective for both classification level and final water resource maps than traditional approaches [20]. Scientists have successfully used MODIS data to map wetlands and coastal zones [36,37,39]. Over the central Congo basin, PALSAR ScanSAR, Envisat altimetry, and MODIS data were used to map the area of wetlands [36]. Using MODIS observations between 2000 and 2010, changes in the inundation of Lake Poyang were monitored [37]. The impact of the dam on the total amount of suspended solids in the Yangtze Estuary and adjacent coastal waters was determined [39] using MODIS data.

The NDWI can be considered a classic index (proposed by Gao in 1996 [55]) that has been tested by many researchers [17,23–29,32,43] for water surface identification and has demonstrated excellent results. The use of Green and NIR channels in the NDWI formula allows for obtaining image resolutions of, respectively, 10 m for Sentinel-2 and 30 m for Landsat-8. Although MODIS covers a scanning area of 2330 km, it has resolutions of 250, 500, and 1000 m, which are not suitable for detailed mapping. Therefore, for this research, using Sentinel-2 and NDVI data was optimal.

Optical data have a wide spectral range, which allows for the identification of numerous objects, including water surfaces and wetlands (with dense vegetation) [17,23–29], but this is dependent on weather conditions; monitoring is not possible on cloudy days. The use of SAR data is not determined by weather conditions (cloudiness); however, the presence of noise complicates processing, and filters are required to eliminate noise [3,4,6]. The use of filters [17] to suppress shadow noise (from SAR data) in urban areas made it possible to effectively highlight large reservoirs and wide riverbeds. As a result [17], it was found that the contrast value according to radar data using the SWI was higher than the value according to optical data using the NDWI.

The ability to penetrate clouds determines the suitability of using Sentinel-1 images for monitoring changes in water bodies. For example, scientists from China [4], using Sentinel-1A/B data and the SNAP platform for image processing, mapped the largest freshwater lake in China, which often suffers from flooding. Often, researchers [2] have compared the results of water surface mapping using different water indices to assess the performance of satellite data. A comparison of Sentinel-1A and Sentinel-2 data for mapping small water bodies in urban and mountainous regions using MNDWI and VH average annual backscatter coefficients (VHavg) showed that MNDWI is more efficient than VH [2]. Using a combination of optical (Landsat-8) and radar (Sentinel-1A) data, researchers [5] managed to carry out the high-frequency monitoring of the ecological state of the same lake for the period ranging from 2015 to 2016.

To improve the Sentinel-1 radar data processing methodology for water surface identification, researchers [3] applied the Lee filter to filter radar noise. They also compared the results of optical data using water indices—the NDWI, MNDWI, a pair of automatic water extraction indices (the AWEI), and radar data—by comparing the polarizations of VV and VH. As a result, the authors of [3] mapped the Bodrog river channel water surface and the characteristics of the indices. The NDWI had the highest error values in populated areas [3]. The disadvantage of using the MNDWI index is its implementation in urban areas with high albedo and a slight deterioration in spatial resolution [3]. The characteristics of the AWEInsh index are relatively successful. Using the AWEIsh and MNDWI indices, areas with high albedo can be considered a significant source of errors. This is because soil, vegetation, and building classes have lower negative values that reflect more SWIR light than green light [3]. Based on the results obtained by these scientists [3], the AWEInsh has relatively successful results, and the NDWI can be used with a mask in populated areas.

The choice of classification method is important in mapping. With the help of Sentinel-2 data based on the NDWI, it was possible [16] to map the open water body of Lake Salda in Turkey. Research has shown [16] that MLC (maximum likelihood classification) provides better results than thresholding methods. The application of classification (MLC) to surface water mapping in several reservoirs in Denmark, Switzerland, Ethiopia, South Africa, and New Zealand helped scientists [26] test a new mapping technique on MNDWI and AWEI data. As a result [26], the classification accuracy of the AWEI became significantly higher in four out of five test sites. Scientists have applied [26] classification (MLC) to Landsat satellite images, which have a resolution of 30 m, but better results can be achieved using Sentinel-2 with a resolution of 10 m or 20 m. The MLC method allows for obtaining results with greater accuracy than the threshold values, which is a significant advantage of the processing technique in our research.

Another important criterion for selecting data is their availability, for example, on the Copernicus Open Access Hub portal. Therefore, we selected Sentinel-1 S1B_IW_GRDH_1SDV and Sentinel-2 S2A/B_MSIL1C data, which are optimal for this research.

When analyzing data from the Climate Change Service (accessed on 1 June 2022, <https://climate.copernicus.eu/hydrological-variables>), the driest months of the year for northeastern Europe were October 2018, September 2019, September 2020, and October 2021. Therefore, in order to avoid the impact of seasonal variations, these periods were chosen for monitoring in this research. Monitoring water bodies in winter, when an ice cover appears, was not performed in this research. For this purpose, other methods (snow indices, filters) should be used. A necessary condition for the use of optical data in this study was the use of a weather filter and the selection of satellite images with 0% cloud cover.

To process the Sentinel-2 multispectral data (Table 1) in order to decipher the water surface of wetlands, the RGB composition was used: SWIR, VNIR, Blue, and NDWI (Band: 3.8) for the water surface only. This is the combination band 11, 8, and 2, which allows for a clear distinction between surface water, arable land, and forest plantations as well as places of urbanization and flooding. Short-wave infrared radiation (SWIR) penetrates $\approx 80\%$ of the atmosphere. As water reflects SWIR light and can absorb near-infrared waves, SWIR measurements allow for the evaluation of how much water is present in soil and plants. By using coefficient values (reflectance values) in the NIR and SWIR bands for the calculations, it is possible to detect the contours of water reservoirs and wet soils.

Table 1. Spectral characteristics of Sentinel-2 images.

Band	Description	Resolution (m)	Central Wavelength (μm)	Wavelength (μm)
Band 1	Coastal Aerosol	60	0.443	0.433–0.453
Band 2	Blue	10	0.490	0.4575–0.5225
Band 3	Green	10	0.560	0.5425–0.5775
Band 4	Red	10	0.665	0.65–0.68
Band 5	Vegetation Red Edge	20	0.705	0.6975–0.7125
Band 6	Vegetation Red Edge	20	0.705	0.7325–0.7475
Band 7	Vegetation Red Edge	20	0.783	0.773–0.793
Band 8	NIR	10	0.842	0.7845–0.8995
Band 8-A	Narrow NIR	20	0.865	0.855–0.875
Band 9	Water Vapor	60	0.945	0.935–0.955
Band 10	SWIR-Cirrus	60	1.380	1.36–1.39
Band 11	SWIR	20	1.610	1.565–1.655
Band 12	SWIR	20	2.190	2.1–2.28

Note: The bands used in the research are highlighted in blue color.

For image classification in this study, we used a supervised classification method (MLC). Thus, according to the data of the RGB composite (band: 11, 8, 2) and the applied classification method (MLC), five types of zones were distinguished:

- 1—Water surface (lakes, rivers, artificial reservoirs);
- 2—Wetlands (waterlogged areas);
- 3—Anthropogenic areas (settlements, human activity places);
- 4—Forest and ecosystems (forests, trees, parks, nature reserves);
- 5—Agricultural land (arable land and land that is actively or periodically used and cultivated—vegetable gardens, fields, and tillage).

Using the developed method for multispectral data using the NDWI helped to identify and map water surfaces, and using RGB composites helped to highlight water surfaces and wetlands that are potential reservoirs. This research was focused on the identification of sites, whereas all other classes were automatically identified (anthropogenic areas, forests, and agricultural lands). The MLC type of classification obtains better results than the thresholding methods [16,26], so the use of MLC classification in this study made it possible to distinguish clear land types and obtain clear boundaries of classified areas.

To identify the surface of water objects (2018–2021) in the driest month of the year according to Sentinel-2 optical data, the NDWI (1) was used, where green is band 3 and NIR is band 8. The NDWI was divided into the categories of certain ranges of index values, interpreted as separate types:

- (1) Water bodies (open water surface) with a range of NDWI values from 0.5 to 1;
- (2) Water bodies, surface water (NDWI from 0.2 to 0.5), and flooding;
- (3) Humidity—NDWI from 0 to 0.2;
- (4) Moderate drought, non-water objects—NDWI from -0.3 to 0;
- (5) Drought, non-water objects—NDWI from -1 to -0.3 .

For most researchers, the study area is a single water object or part of the water area. In our case, the study area is about 26,000 km² and has contrasting terrain and different types of areas. Therefore, it is necessary to use filters for generating classification types (unification), removing areas that are too small, and smoothing boundaries. This was carried out at the stage of post-classification processing with the help of the following options: combination (region group), majority generation (majority filter), increasing the clarity of boundaries, and removing areas that were too small. Then, the obtained data (maps) were stratified for the detailed selection and calculation of areas of interest, and a description of the obtained results was prepared.

When using radar data to identify water surfaces, it is imperative to use noise reduction filters. The use of speckle filtering (Lee filter) to identify water surfaces is common in modern research when processing satellite images containing radar data in the SNAP program [1,3,4,6,48]. Speckle filters are moving window filters that change the value of the central pixel based on all pixel values in the window. There are the different window sizes— 3×3 , 5×5 , and 7×7 —and, in this research, we used a 5×5 window. The window size, along with the resolution, affects the quality (the sharpness of the boundaries) of the image. All window sizes were tested for the study area. The optimal result was obtained with a window size of 5×5 ; the identified water surfaces had clear boundaries and better filtration results. A sigma filter preserves image sharpness and detail while suppressing noise (Lee filter). In addition to the Lee speckle filter, it was necessary to apply other filters such as terrain correction, terrain flattening, and thermal noise removal, which correct for errors in the raster and geocoding and absorb thermal noise.

SAR data processing can be divided into several stages. The stages of the SAR data processing methodology can be seen in Figure 2. At the first stage, we downloaded Sentinel-1 data from the Copernicus Open Access Hub. It is best to use the S1B_IW_GRDH_1SDV product as it already has been pre-processed, then use SNAP to process the image, followed by the calibration and application of filters (terrain flattening and terrain correction), the removal of thermal noise, and the application of a sigma filter (Lee filter) to suppress noise. The main stages of the method applied to process the optical and radar data are shown in Figure 2.

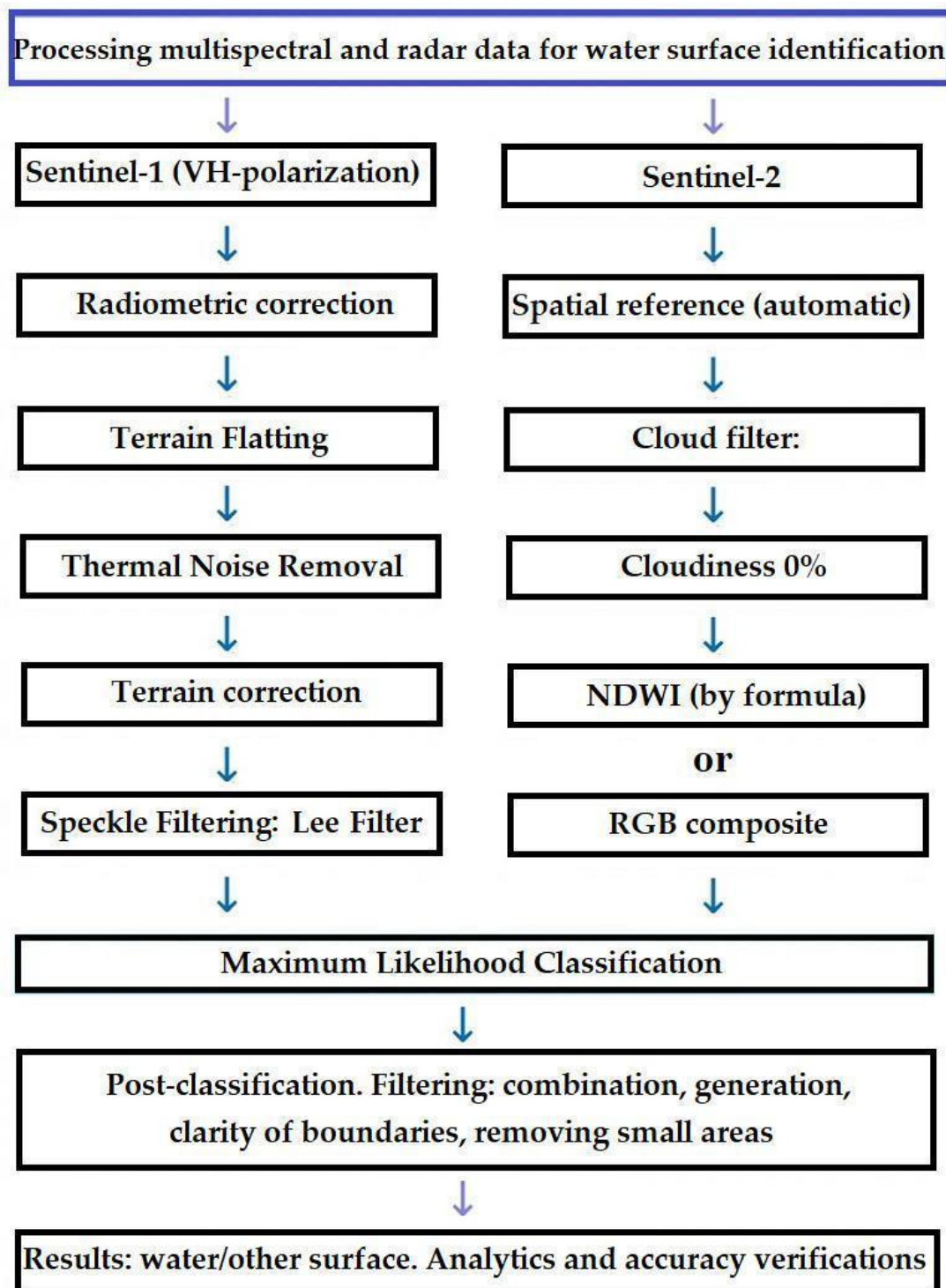


Figure 2. Schematic diagrams of the proposed methodology of remote sensing multispectral (Sentinel-2) and SAR data (Sentinel-1) processing for water surface identification.

To test the described processing method on a test area of 1611 km², the mapping of water surfaces and wetlands was carried out using Sentinel-2 multispectral data (RGB:11, 8, 2), as shown in Figure 3. The raster image clearly visualizes the water surface.

At the next stage of the research, using the described processing methodology with MLC classification and the use of the NDWI for Sentinel-2, we mapped the water and other surfaces on the test area (Figure 4a) and, as a result of the classification (Figure 4b), obtained clear boundaries of water areas (Figure 4c).

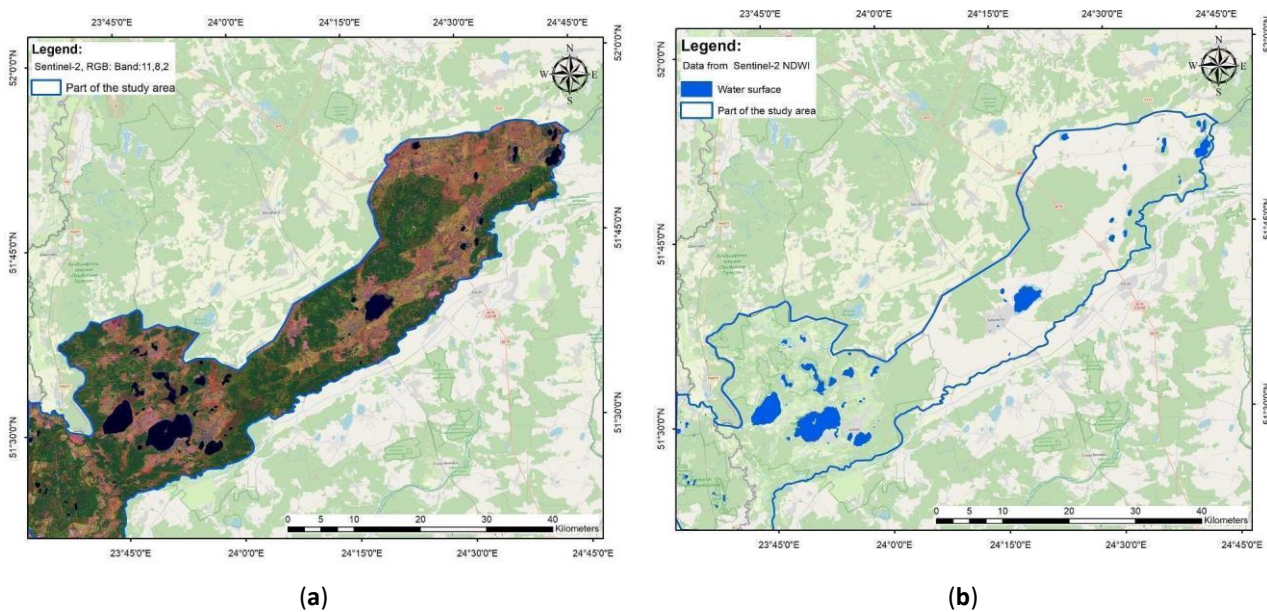


Figure 3. Maps of identified water surfaces at the test area, obtained from Sentinel-2A/B data at the test area of 1,611 km². (a): Composite band RGB:11, 8, 2; (b): water surfaces (results obtained).

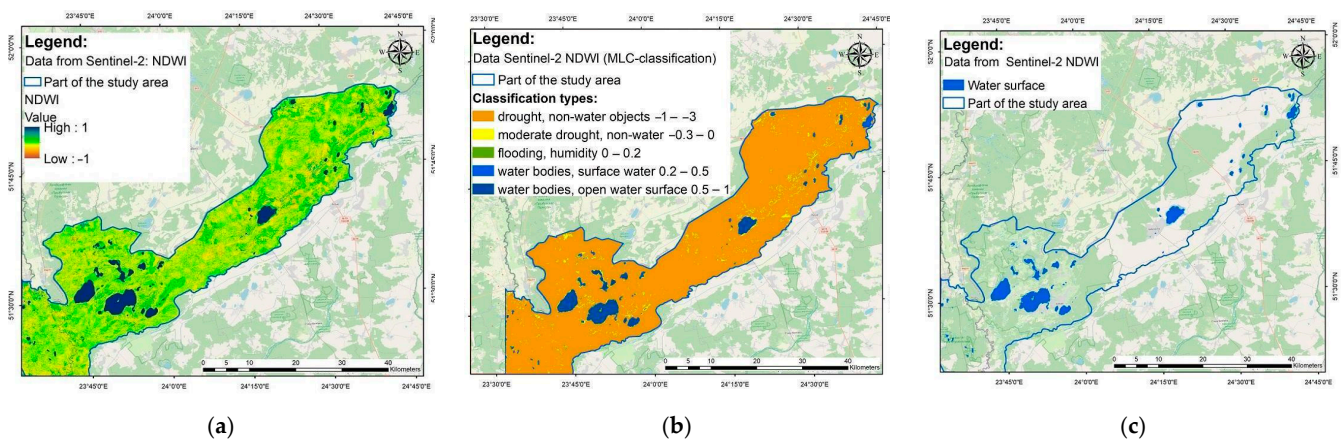


Figure 4. Maps of the identified water surfaces in the test area based on Sentinel-2A/B data at the test area: (a) map with NDWI; (b) map with area classification; (c) map with water surfaces (results obtained).

By using SAR data with VH polarization and applying the Lee filter methodology (Figure 5a), the result was water surfaces (Figure 5b) with clear boundaries and accurate raster data mapping.

Analyzing the parameters of SAR data (Sentinel-1 with VH polarization) and scientific research by various authors [1–7,45–47,52], values from 0 to 0.009 were used to identify water surfaces based on VH polarization data; the identified water surfaces on the test site are shown in Figure 5a.

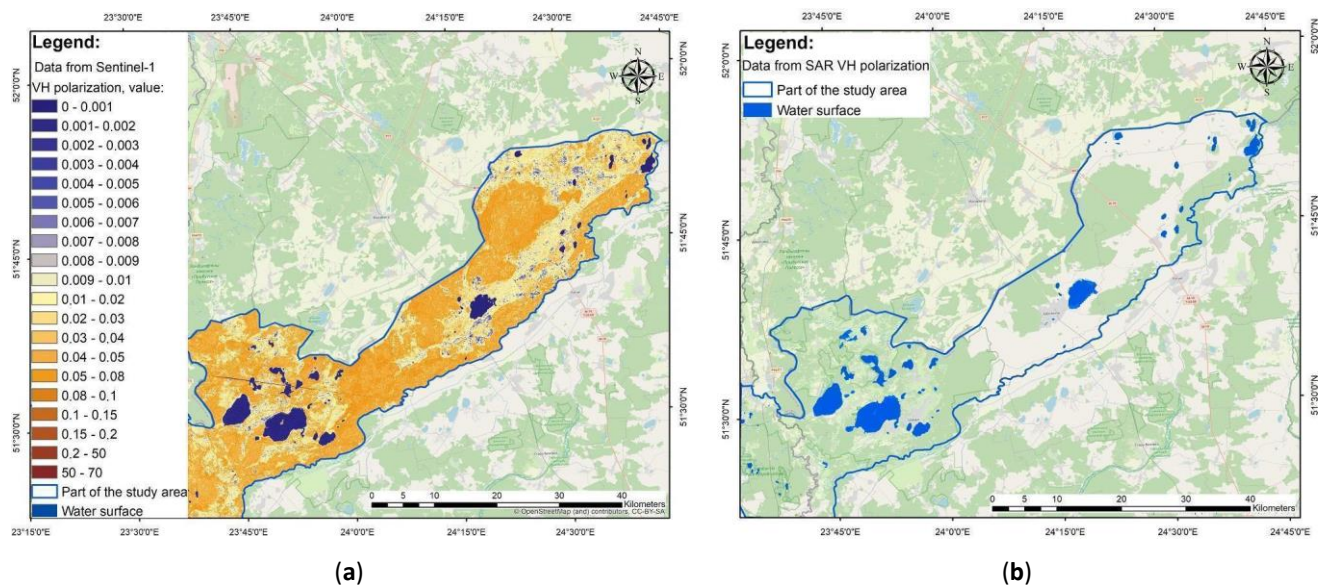


Figure 5. Maps of identified water areas on the test area using SAR data with VH polarization (Lee filter) at the test area: (a) map with classification; (b) map with water surfaces (results obtained).

Classification Accuracy Evaluation—Kappa Coefficient

Generally, the visualization of the comparison of identified water surfaces demonstrates the identity of the results obtained; however, to verify the reliability of the results obtained, it is necessary to perform a procedure for assessing the accuracy of the method applied. For this purpose, the Kappa coefficient (or confusion matrix) was calculated, which is a popular measure used by many scientists to obtain the statistical percentage of the results [1–6,17,18,28,33,48] to determine the accuracy of image classification based on remote sensing data for multispectral and SAR data.

In addition to the Kappa coefficient itself, the following statistical accuracy indicators can also be calculated: PA—producer accuracy (5), UA—user accuracy (6), and OA—overall accuracy (7). The output result “TN” stands for “True Negative”, which shows the number of negative examples that were classified accurately. “TP” stands for “True Positive”, which indicates the number of positive examples that were classified correctly. The term “FP” indicates the False Positive rate, meaning the number of actual negative examples that were classified as positive, while “FN” indicates the False Negative rate [3,4]:

$$PA = TP / (TP + FN), \quad (5)$$

$$UA = TP / (TP + FP), \quad (6)$$

$$OA = (TP + TN) / T, \quad (7)$$

The Kappa coefficient (8) is a comparative calculation of predicted and actual values (a comparison of the final pixels with a reference background image). In our example, we visually compared a Maxar image from the Google Earth Pro platform with the existing images.

The predicted values include the observation points that we placed on the obtained maps with classified types—water, non-water surfaces (for Sentinel-1), water surfaces, wetlands, and other classes (for Sentinel-2)—which were provided according to the categorization. Then, using Google Earth Pro technology, the classified values were recorded and compared with the actual values. And, using Formula (8), the Kappa accuracy coefficient was calculated.

$$Kappa = [T \times (TP + TN) - [(TP + FP) \times (TP + FN) + (FN + TN) \times (FP + TN)]] / TP + FN, \quad (8)$$

For the test area, where the largest number of water bodies is located, the Kappa accuracy coefficient was calculated using 40 observation points located on all water bodies and other classes, as presented in Figure 6.

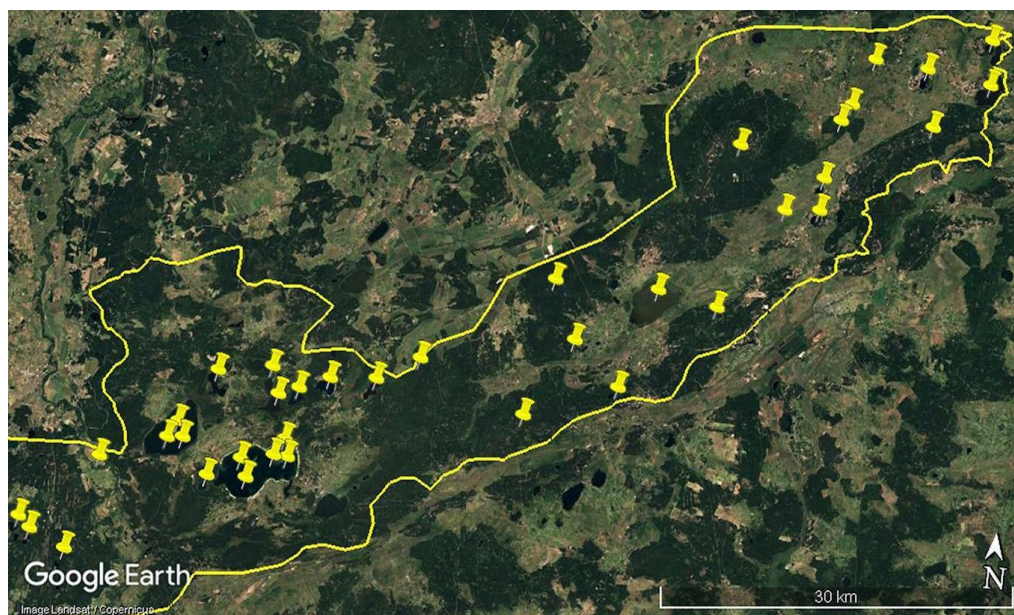


Figure 6. A map of the location of the observation points to measure the accuracy of the data obtained at the test area.

The results of the accuracy calculations of the Kappa coefficient based on optical and radar data are presented in Table 2.

Table 2. Accuracy estimates of water body detection based on SAR data with VH polarization (using the Lee filter) and multispectral data with MLC classification.

Data Product (Sensing Date)	Processing Data	Spatial Resolution	S Water Surface, Thousand km ²	PA Water Surface	UA Water Surface	OA	Kappa %
S2B_MSIL1C 2018.10.14	RGB:11, 8, 2 + MLC	20 m	92.56	1.0	0.84	0.88	84.95
S2B_MSIL1C 2018.10.14	NDWI + MLC	10 m	76.45	0.87	1.0	0.90	85.88
S1B_IW_GRDH_1SDV 2018.10.11	VH + Filters + MLC	10 m	76.78	1.0	0.94	0.94	88.84

According to the results of their methods, most researchers [3,4,6,33] obtained accuracy rates for SAR data ranging from 73% to 89% and for optical data from 50% to 96% [3]. In the present research, the Kappa coefficient for SAR data with VH polarization was obtained at the test site at 88.84%; for multispectral data, the NDWI (with MLC classification) and Kappa coefficient were 84.95% and 85.88%, which indicates the high accuracy of the methodology used and the prospects of its application for identifying water surfaces.

The results (Table 2) show a difference in the total water surfaces obtained from Sentinel-2 data with RGB composite (band: 11, 8, 2), Sentinel-1 (VH polarization), and the NDWI (band: 3, 8). This difference is due to the use of different spectral bands. For RGB, these are 1.565–1.655 μm , 0.7845–0.8995 μm , and 0.4575–0.5225 μm . The sensitivity of the spectra in this composition allows us to identify water bodies with different depths and wetlands. For example, during a drought, wetlands can be observed in places where there were previously water bodies, which are clearly recorded on images with this composition.

To calculate the NDWI for Sentinel-2, the formula uses bands 3 and 8 with spectra 0.5425–0.5775 and 0.7845–0.8995. The use of the NDWI and SAR data determines open water surfaces and their allocation against the background of soil and vegetation, so small wetlands with shallow depths are not recorded using these data.

The obtained high accuracy indicators for the determination of water surfaces and wetlands in the test area allow for the use of applicable methods and data, such as the NDWI; composite band 11, 8, 2; and VH polarization (with filters) with MLC classification for the entire study area, including the basins of the Bug, Dniester, and San rivers themselves.

4. Results

For the first time, using the developed method, the areas of the Bug, Dniester, and San river basins were mapped using remote sensing optical and radar data, with the selection of the water surface and wetlands.

Sentinel-1 radar data with VH polarization using the Lee speckle filter to identify water layers were used experimentally [2–4,6,17] to study one water object. In our case, the research area has a large number of water bodies and many small areas of various types; in addition, it is necessary to eliminate noise. Therefore, the developed technique (described in Section 3) included the options necessary for removing thermal noise: terrain flattening, terrain correction, thermal noise removal, relief correction, and Lee speckle filter. Regarding the generalization and removal of very small areas, this was solved at the stage of post-classification processing, which included a majority filter, boundary clean, and region group.

Using the developed method for multispectral data using the NDWI (described in Section 3) helped to identify and map water surfaces and using RGB composites aided in highlighting water surfaces and wetlands that are potential reservoirs. This research was focused on the identification of sites, while all other classes were automatically identified (anthropogenic areas, forests, and agricultural lands). The use of MLC classification in this study made it possible to distinguish clear types of land and obtain clear boundaries of classified areas.

As a result, maps were built with the selection of water surfaces for each river basin based on radar Sentinel-1 and optical Sentinel-2 data with the calculation of water areas and the assessment of the accuracy of the Kappa coefficient, PA, UA, and OA. The results are presented below.

4.1. Identification of the Water Surface and Wetlands of the Bug River Basin Using Remote Sensing Data

4.1.1. The Identification of the Water Surface and Wetlands of the Bug River basin Using Multispectral Data: RGB Composite with MLC Classification

The methodology used for Sentinel-2 optical data, with an RGB composition of bands 11, 8, and 2 and MLC classification, allows for distinguishing the following classification areas: water surfaces, wetlands, anthropogenic areas, forests and ecosystems, and agricultural land within the Bug River basin. As a result, an RGB composite (bands 11, 8, and 2) was created and a map with these types of sites for the Bug River basin was obtained, as shown in Figure 7.

The Bug River basin occupies an area of 15,000 km². According to the received data, the plots with an open water surface occupy 150 km², and wet plots (wetlands) are 435 km², which make up about 1% and 2.8%, respectively; the latter areas are concentrated in the river valleys and around the lakes. By using this methodology with the sensitive spectral bands of the applied RGB composition, it was possible to successfully identify wetland and water surfaces. But, at the next stage of the study, we decided to use the NDWI with MLC classification to identify open water surfaces.

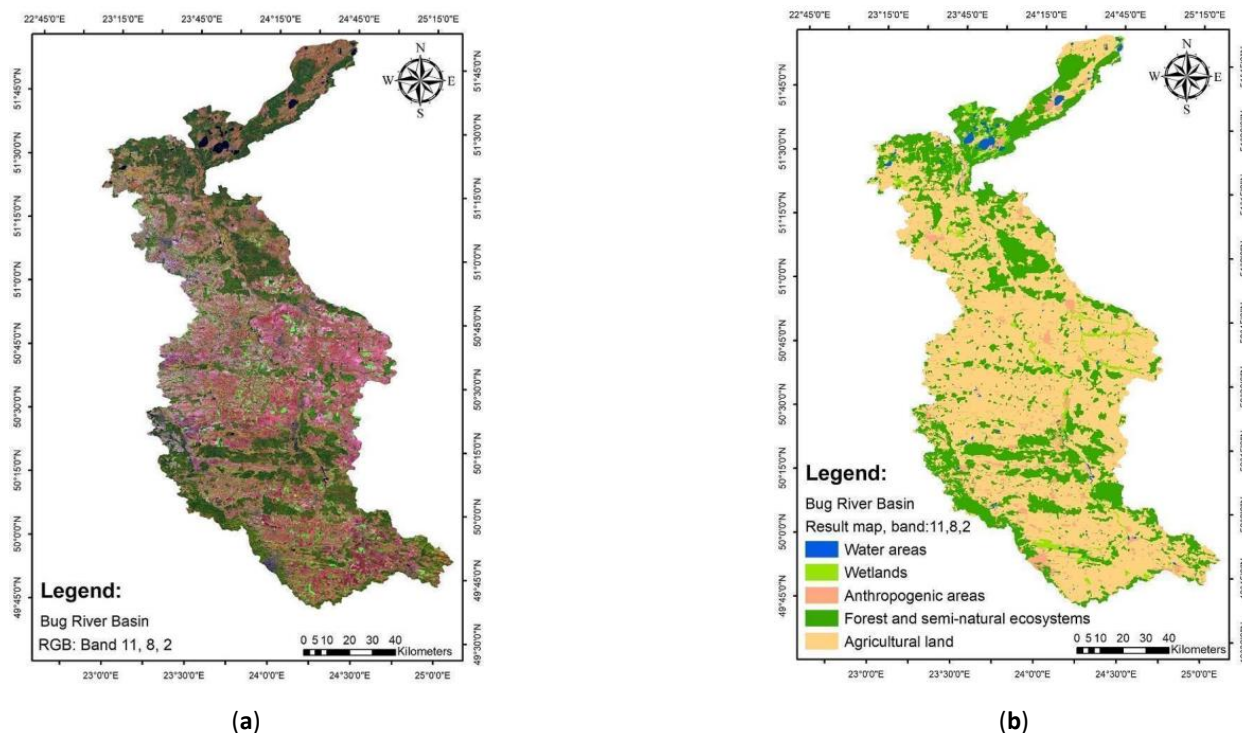


Figure 7. Maps of the Bug River basin created based on multispectral Sentinel-2 data. (a): RGB composite map with spectral bands 11, 8, and 2. (b): The results map of the classified area types using the MLC classification method.

4.1.2. The Identification of the Water Surface of the Bug River Basin Using Multispectral Data: NDWI with MLC Classification

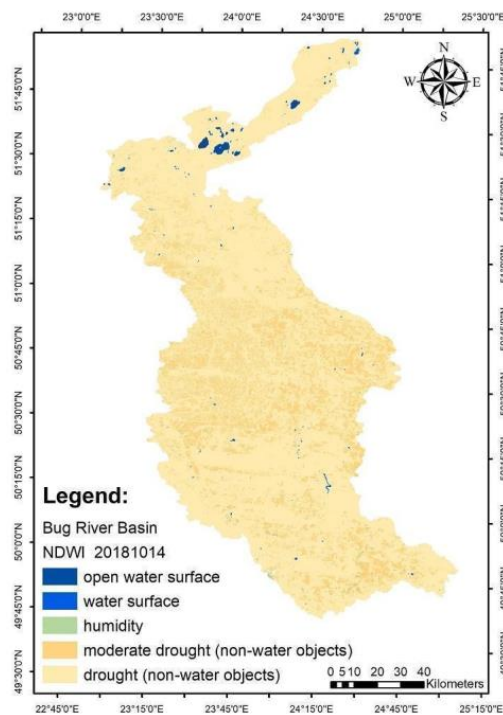
Using the Sentinel-2 multispectral data and the NDWI (with MLC classification), we identified and monitored changes in water surfaces. The monitoring of changes in open water surfaces during the driest period (month) of the year was carried out in the territory of the Bug River basin from 2018 to 2021 using NDWI data.

On the map of the Bug River basin obtained from the NDWI data, open water surfaces were identified in different periods, and their changes are shown in Figure 8a–d.

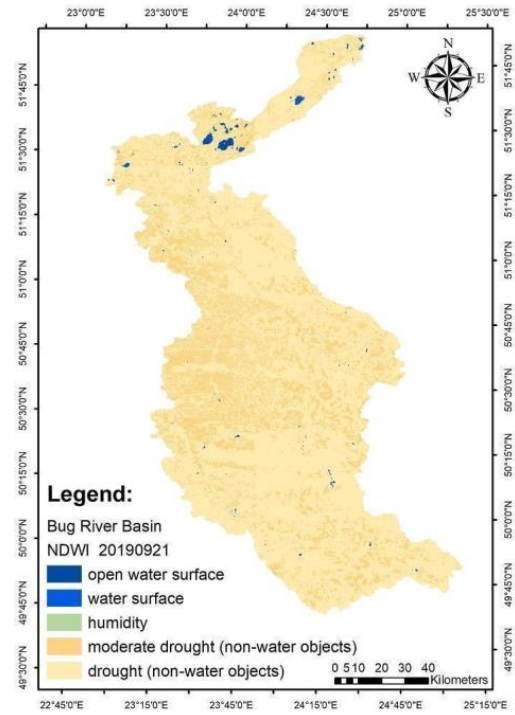
The categorization of moderate drought (non-water objects)—NDWI from 0.3 to 0—and drought (non-water objects)—NDWI from -1 to -0.3 —has been accomplished; therefore, their division into small subcategories such as forest, field, and mountains is not necessary, as attention has mainly been given to the identification of the water surface and water objects.

To determine the accuracy (reliability) of the constructed maps with water surfaces, the Kappa coefficient was calculated. These maps have been applied to calculate the areas of water surfaces ($S_{\text{Water Surface}}$) and to calculate the statistical indicators of measurement accuracy, the Kappa coefficient, PA—producer accuracy, UA—user accuracy, and OA—overall accuracy, which are shown in Table 3. In calculating the Kappa coefficient from the maps, around 100 observation points were created across the Bug River basin.

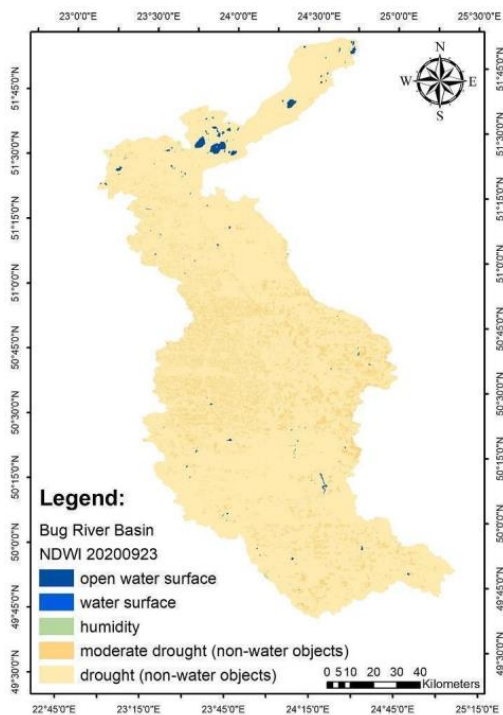
According to the NDWI data, in the Bug River basin, the largest values (areas) of water surface were recorded in 2021 at 102.58 thousand km² and in 2018 at 102.24 thousand km², which are shown in Table 3. This indicates that in this area, 2018 and 2021 were wetter than 2019 and 2020. The accuracy values obtained from the Kappa coefficient for the Bug River basin are quite high and range between 76.07 and 85.88%. The recorded statistical indicator, UA, of the water surface ranges from 0.92 to 1, which shows the high quality of the user's accuracy procedure.



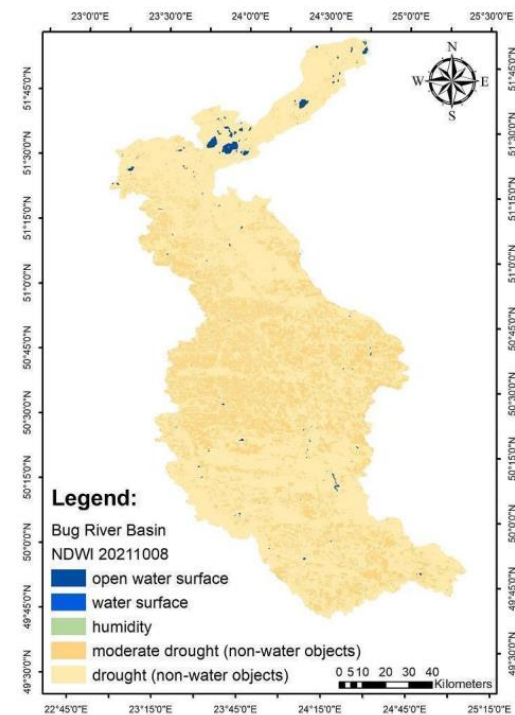
(a)



(b)



(c)



(d)

Figure 8. Maps of the Bug River basin created based on multispectral Sentinel-2 data using the NDWI and MLC classification. Map of classified area types based on NDWI data for the dry season: (a) October 2018, (b) September 2019, (c) September 2020, and (d) November 2021.

Table 3. The results of the accuracy assessment of the obtained classified maps of the Bug River basin using NDWI data.

Product Data (Sensing Date)	Spatial Resolution	S Water Surface, thousand km ²	PA Water Surface	UA Water Surface	OA	Kappa %
S2B_MSIL1C_ 2018.10.14	10 m	102.24	0.87	1.0	0.91	85.88
S2B_MSIL1C_ 2019.09.24.	10 m	99.82	0.73	0.96	0.9	79.54
S2B_MSIL1C_ 2020.09.23.	10 m	98.38	0.72	1.0	0.84	76.71
S2B_MSIL1C_ 2021.10.05.	10 m	102.58	0.75	0.92	0.86	79.86

4.1.3. The Identification of the Water Surface of the Bug River Basin Using SAR Data: VH Polarization with MLC Classification

Then, using the described methodology, we built maps with water surfaces using SAR data with VH polarization and MLC classification; the result is shown in Figure 9a–d.

The Kappa coefficients for maps prepared for the Bug River basin based on SAR data with VH polarization and MLC classification range from 87.61 to 93.43%, as shown in Table 4, and are higher than the results from optical data. The quality of the user's accuracy procedure is shown by the UA index of the water surface, which ranges from 0.91 to 0.95. In calculating the Kappa coefficient for the maps, around 100 observation points were involved (see Table 4).

According to the SAR data obtained in the Bug River basin, the largest values of the water surface area were recorded in 2021 at 109.31 thousand km² and in 2018 at 108.37 thousand km², which are shown in Table 4. This indicates that 2018 and 2021 were wetter than 2019 and 2020, and the same results were obtained according to the NDWI data.

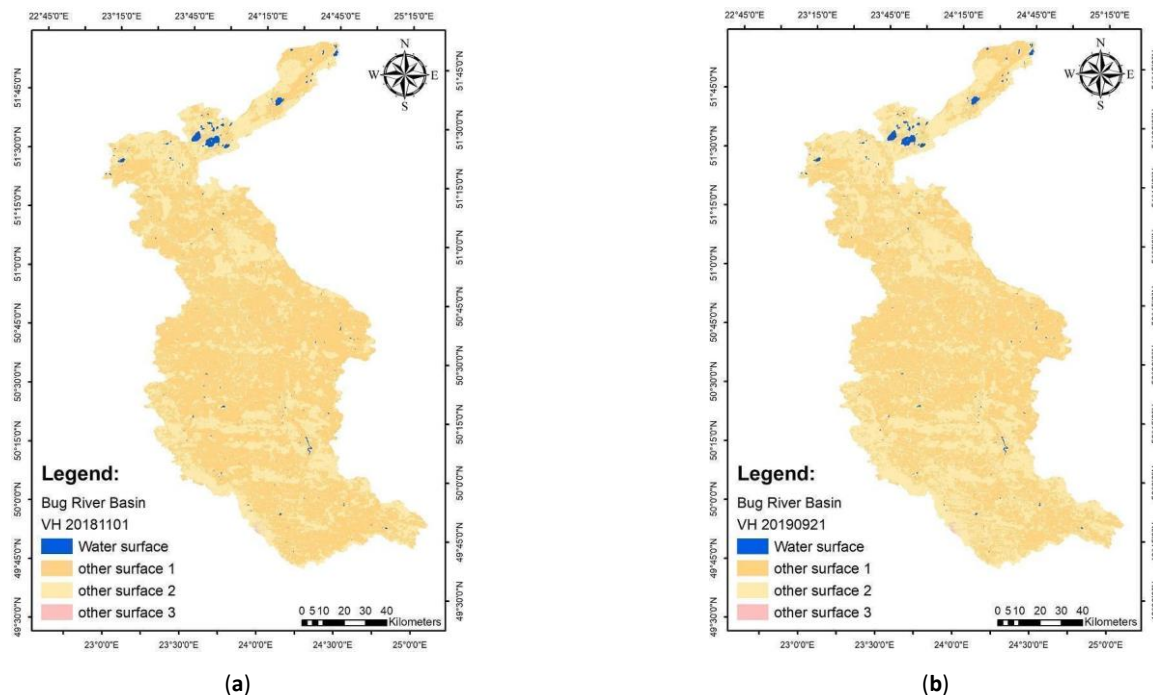


Figure 9. Cont.

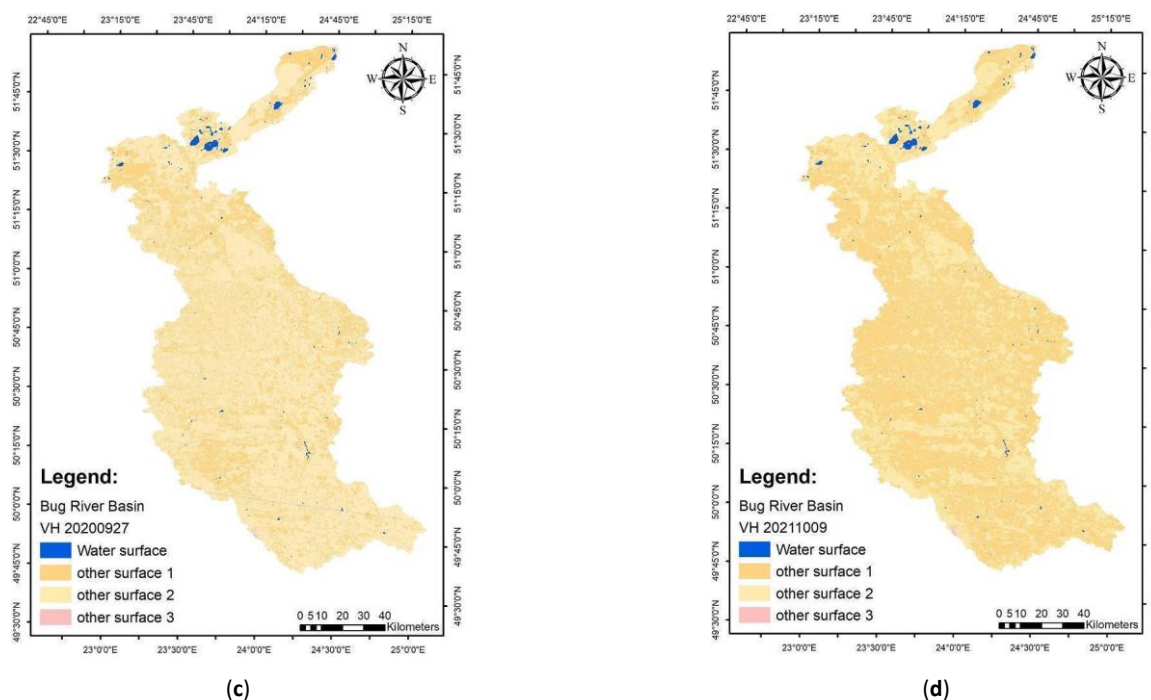


Figure 9. Maps of the Bug River basin created using Sentinel-1 (SAR) data and using filters (Lee) and MLC classification. Map of classified area types based on VH polarization data for the dry season: (a) November 2018, (b) September 2019, (c) September 2020, and (d) October 2021.

Table 4. The results of the accuracy assessment of the obtained classified maps of the Bug River basin using SAR data (Sentinel-1).

Product Data (Sensing Date)	Spatial Resolution	S Water Surface, thousand km ²	PA Water Surface	UA Water Surface	OA	Kappa %
S1B_IW_GRDH_1SDV_ 2018.10.11	10 m	109.31	1.0	0.93	0.95	93.37
S1B_IW_GRDH_1SDV_ 2019.09.21.	10 m	107.41	1.0	0.87	0.93	90.52
S1B_IW_GRDH_1SDV_ 2020.09.27.	10 m	107.01	0.94	1.0	0.91	87.61
S1B_IW_GRDH_1SDV_ 2021.10.04.	10 m	108.37	1.0	0.94	0.95	93.43

In conclusion, high statistical accuracy rates were obtained for the Bug River basin using SAR data, which indicates the reliability of the measurements of the allocated water areas and the prospects for its application in this area.

The obtained measurement accuracy indicators demonstrate the feasibility of applying this methodology (using SAR data with VH polarization) for mapping water surfaces over large areas.

4.2. The Identification of the Water Surface and Wetlands of the Dniester River Basin Using Remote Sensing Data

4.2.1. The Identification of the Water Surface and Wetlands of the Dniester River Basin Using Multispectral Data: RGB Composite with MLC Classification

The Dniester River basin covers a much smaller area than the Bug, with a surface area of around 6000 km². Similarly to the Bug River basin, the following classification areas were identified using Sentinel-2 optical data processing with an RGB composition of bands 11, 8, and

2 and MLC classification: water surface, wetlands, anthropogenic areas, forests and ecosystems, and agricultural land within the Dniester River basin, as shown in Figure 10.

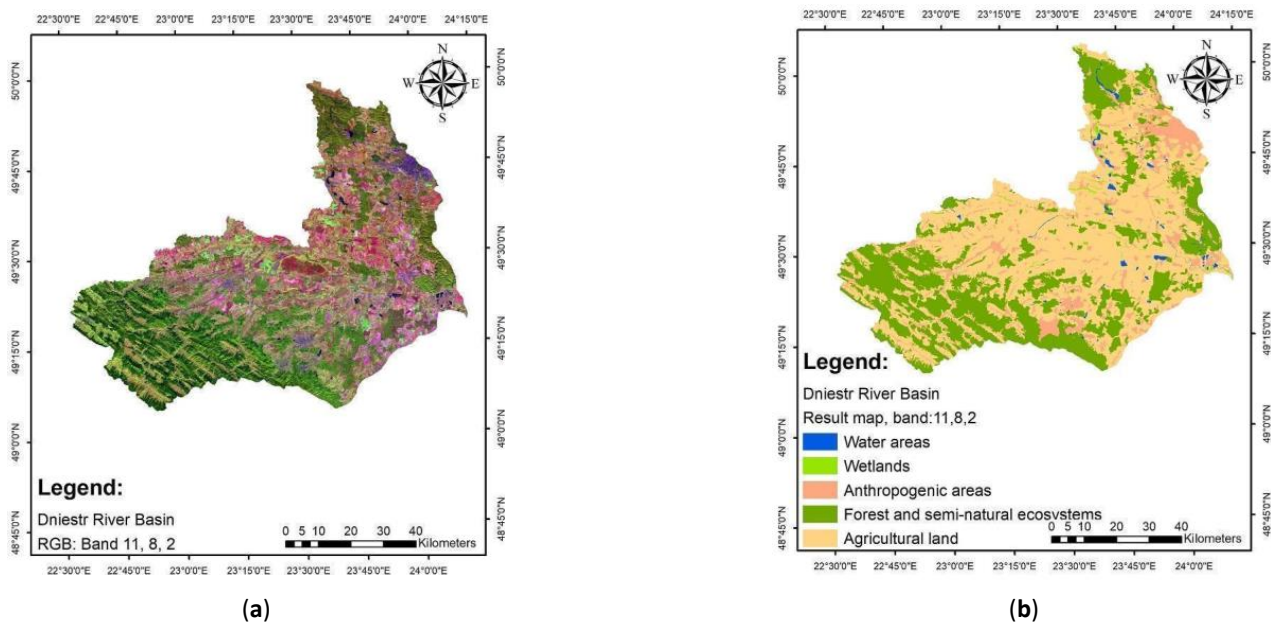


Figure 10. Maps of the Dniester River basin created using multispectral Sentinel-2 data. (a): RGB composite map with spectral bands 11, 8, and 2. (b): The results map of classified area types using the MLC classification method.

4.2.2. The Identification of the Water Surface of the Dniester River Basin Using NDWI, Composite with MLC Classification

At the next stage of the research, the NDWI with MLC classification was applied to build maps with water and other surfaces in the Dniester River basin (see Figure 11).

When analyzing the maps created for the 2018–2021 dry period, changes in the water surface can be observed; for example, in 2018 (Figure 11a), the water surface was approximately 21.05 thousand km², and in 2020, it was around 18.18 thousand km².

In calculating the Kappa coefficient, around 80 observation points were obtained. The areas of identified water surfaces and the measurement accuracy in the Dniester River basin are presented in Table 5.

Table 5. The results of the accuracy assessment of the obtained classified maps of the Dniester River basin using NDWI data.

Product Data (Sensing Date)	Spatial Resolution	S _{Water Surface} , thousand km ²	PA Water Surface	UA Water Surface	OA	Kappa %
S2B_MSIL1C_2018.10.14.	10 m	21.05	0.9	1.0	0.91	87.25
S2B_MSIL1C_2019.10.14.	10 m	19.72	0.8	0.8	0.88	83.03
S2B_MSIL1C_2020.09.10.	10 m	18.18	0.8	1.0	0.85	79.76
S2B_MSIL1C_2021.08.10.	10 m	19.46	0.86	1.0	0.88	82.61

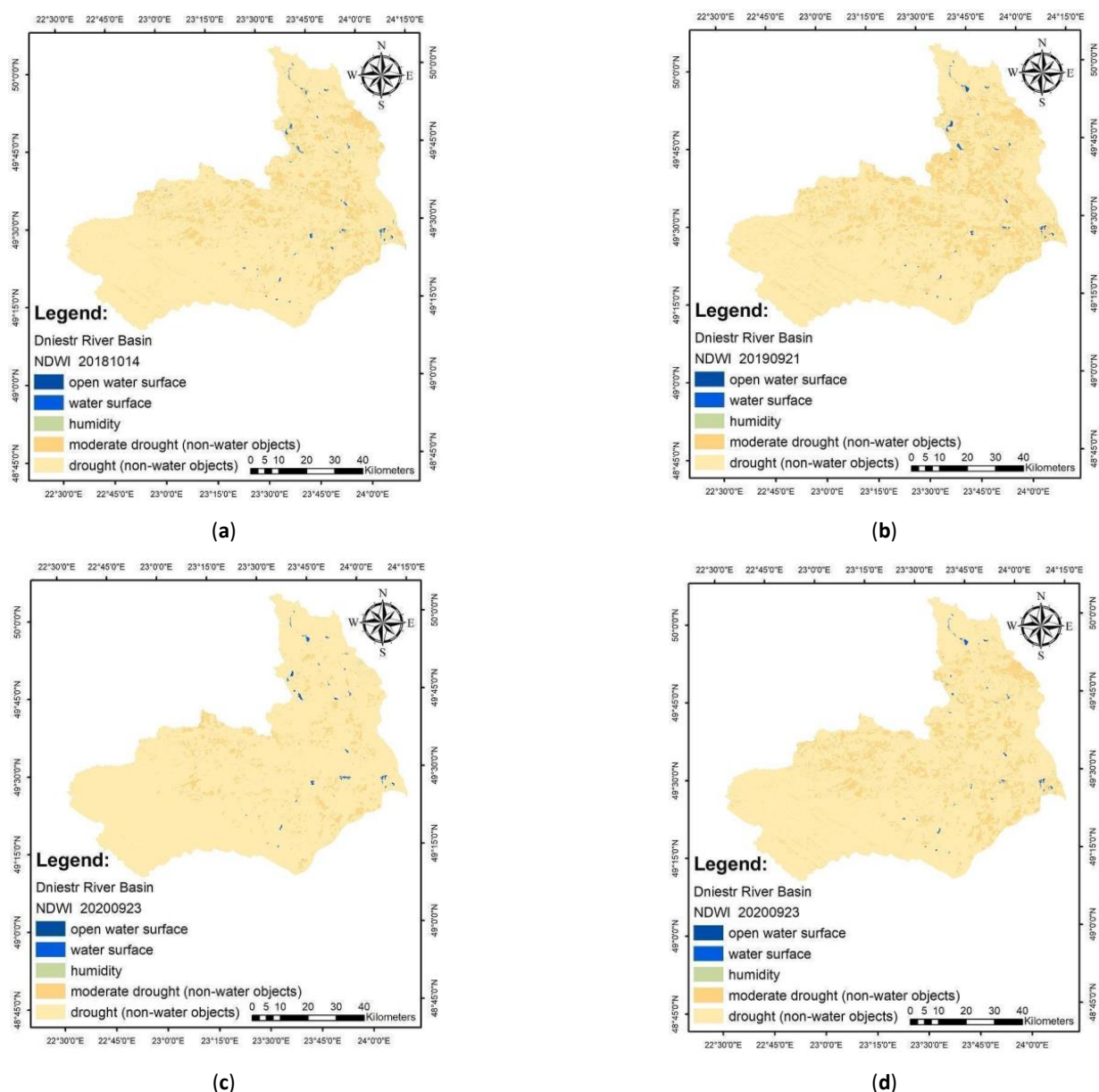


Figure 11. Maps of the Dniester River basin created on multispectral Sentinel-2 data using NDWI and MLC classification. Map of classified area types based on NDWI data for the dry season: (a) October 2018, (b) September 2019, (c) September 2020, and (d) November 2021.

According to the NDWI data, in the Dniester River basin, the largest values of water surface area were recorded in 2021 at 21.05 thousand km² and in 2019 at 19.72 thousand km², which are shown in Table 5. This indicates that 2018 and 2019 were wetter (according to the NDWI) compared with 2020 and 2021. The measurement accuracy of the Kappa coefficient is from 79.76% to 87.25%, which represents a perspective result based on remote sensing data using this processing method. However, to obtain accurate data on the drought/wetting trends, monitoring is required at 3–5-day intervals over several months.

4.2.3. The Identification of the Water Surface of the Dniester River Basin Using SAR Data: VH Polarization with MLC Classification

The next stage was to obtain maps of the Dniester River basin area with water surface areas based on SAR data (with VH polarization) and MLC classification using the described

methodology and to assess the accuracy of the results. As a result, the SAR data were used to generate maps of different periods, as shown in Figure 12.

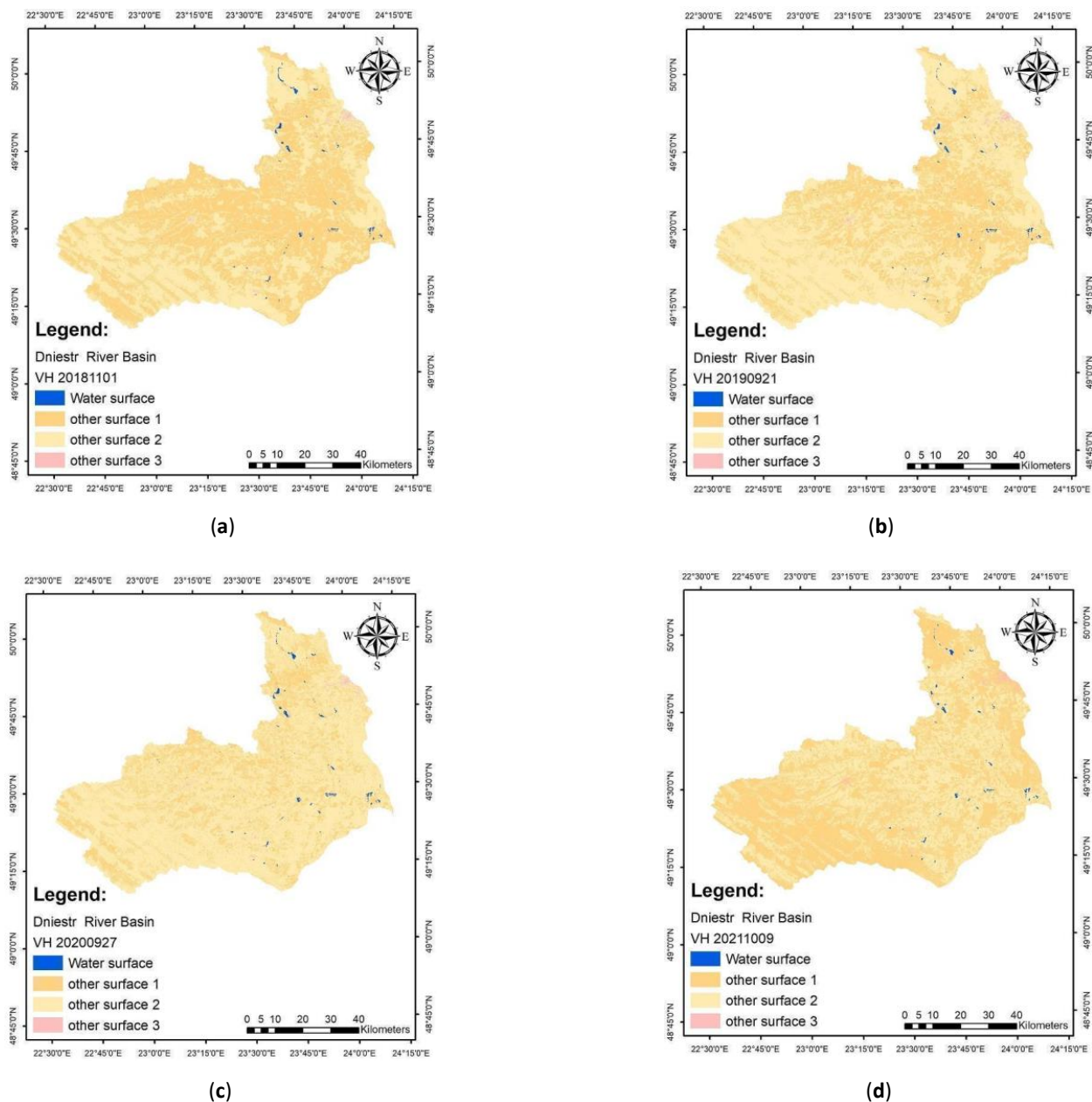


Figure 12. Maps of the Dniester River basin created using Sentinel-1 (SAR) data and using filters (Lee) and MLC classification. Map of classified area types based on VH polarization data for the dry season: (a) November 2018, (b) September 2019, (c) September 2020, and (d) October 2021.

After performing the accuracy measurement procedure, we obtained data with Kappa coefficients of 91.41% to 97.18%, which is higher than the multispectral data for this part of the Dniester River basin. Approximately 80 observation points were considered when calculating the Kappa coefficient. The results of the accuracy and area measurements are shown in Table 6.

According to the SAR data, in the Dniester River basin, the largest values of water surface area were recorded in 2020 at 22.86 thousand km² and in 2018 at 20.75 thousand km², which are shown in Table 6. This indicates that, according to SAR data, 2018 and 2020 were wetter than 2019 and 2021.

Table 6. The results of the accuracy assessment of the obtained classified maps of the Dniester River basin using SAR data (Sentinel-1).

Product Data (Sensing Date)	Spatial Resolution	S Water Surface, thousand km ²	PA Water Surface	UA Water Surface	OA	Kappa %
S1B_IW_GRDH_1SDV_2018.10.16.	10 m	20.75	1.0	0.94	0.98	97.18
S1B_IW_GRDH_1SDV_2019.09.21.	10 m	20.52	1.0	1.0	0.96	94.9
S1B_IW_GRDH_1SDV_2020.09.27.	10 m	22.86	1.0	1.0	0.93	91.41
S1B_IW_GRDH_1SDV_2021.10.04.	10 m	19.17	0.88	1.0	0.96	95.17

4.3. The Identification of the Water Surface and Wetlands of the San River Basin Using Remote Sensing Data

4.3.1. The Identification of the Water Surface and Wetlands of the San River Basin Using Multispectral Data: RGB Composite with MLC Classification

As a result of mapping, the construction of RGB composite (bands 11, 8, and 2), and the use of the above method for the territory of the San River basin, a map of the basin with the selected types of sites was developed, as presented in Figure 13a,b.

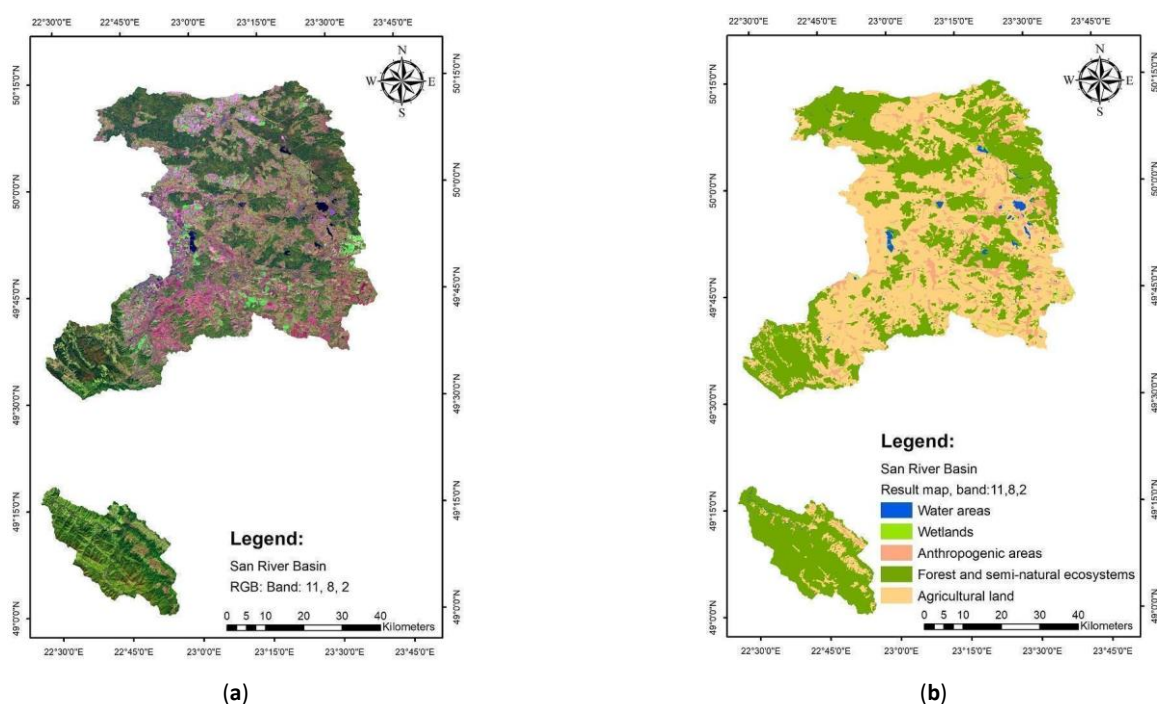


Figure 13. Maps of the San River basin created based on multispectral Sentinel-2 data. (a) RGB composite map with spectral bands 11, 8, and 2. (b) The results map of classified area types using the MLC classification method.

The San River basin occupies an area of approximately 4550 km². Using the obtained data, it has been established that the area of open water surface is 37.06 km² while wetlands constitute 30.03 km², or about 0.82% and 0.66%, respectively. The data obtained generally reflect the ratio of water surface, wetlands, and other categories of land found in the San River basin. However, to update data on changes in water bodies, it is necessary to conduct monitoring at a certain frequency.

4.3.2. The Identification of the Water Surface of the San River Basin Using Multispectral Data: NDWI with MLC Classification

At the next stage of the research, the NDWI was used to build maps with water surfaces in the San River basin area using MLC classification for the dry period of 2018–2021; the results of this mapping are shown in Figure 14a–d.

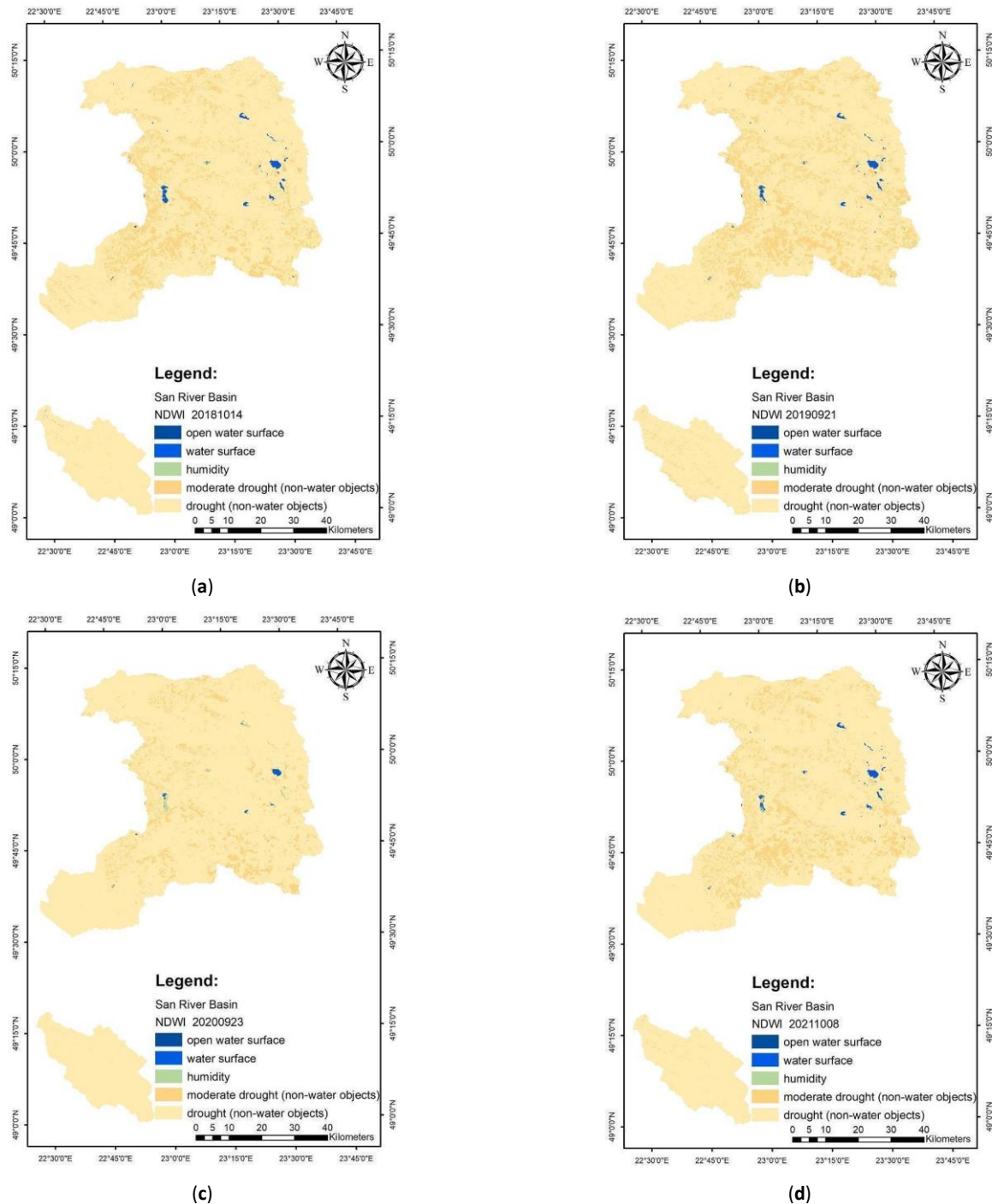


Figure 14. Maps of the San River basin created using multispectral Sentinel-2 data and using the NDWI and MLC classification. Map of classified area types based on NDWI data for the dry season: (a) October 2018, (b) September 2019, (c) September 2020, and (d) November 2021.

While calculating the Kappa coefficient for the maps, around 80 observation points were created throughout the San River basin.

The accuracy of the Kappa coefficient measurements ranges from 76.28% to 88.65%, which is a perspective result obtained from multispectral data for a territory of over 1000 km².

The areas of identified water surfaces and the measurement accuracy in the Dniester basin are presented in Table 7.

Table 7. The results of the accuracy assessment of the obtained classified maps of the San River basin using NDWI data.

Product Data (Sensing Date)	Spatial Resolution	S Water Surface, thousand km ²	PA Water Surface	UA Water Surface	OA	Kappa %
S2B_MSIL1C_ 2018.10.14.	10 m	24.59	0.7	1.0	0.82	77.05
S2B_MSIL1C_ 2019.10.14.	10 m	22.42	0.7	1.0	0.82	84.15
S2B_MSIL1C_ 2020.09.21.	10 m	20.67	0.92	1.0	0.91	88.65
S2B_MSIL1C_ 2021.10.08.	10 m	20.47	0.83	1.0	0.82	76.28

According to the NDWI data, in the San River basin, the largest values of water surface area were recorded in 2018 at 24.59 thousand km² and in 2019 at 22.42 thousand km², which are shown in Table 7. This indicates that 2018 and 2019 were wetter (according to the NDWI) compared with 2020 and 2021.

4.3.3. The Identification of the Water Surface of the San River Basin Using SAR Data: VH Polarization with MLC Classification

Following the described methodology, based on the SAR data (with VH polarization) with the use of filters (including the Lee filter) and MLC classification, maps of the San River basin were created with identified water surface areas. The results of mapping in the San River basin, according to SAR data by year, are shown in Figure 15 ((a) 2018, (b) 2019, (c) 2020, and (d) 2021).

After performing the accuracy measurement procedure, data with Kappa coefficients of 91.41% to 97.18% were obtained, which is higher than the multispectral data for this area; all results of the accuracy and area measurements are shown in Table 8.

Table 8. The results of the accuracy assessment of the obtained classified maps of the San River basin using SAR data (Sentinel-1).

Product Data (Sensing Date)	Spatial Resolution	S Water Surface, thousand km ²	PA Water Surface	UA Water Surface	OA	Kappa %
S1B_IW_GRDH_1SDV_ 2018.10.16.	10 m	23.62	1.0	1.0	0.94	92.43
S1B_IW_GRDH_1SDV_ 2019.09.21.	10 m	23.14	0.98	0.93	0.94	92.87
S1B_IW_GRDH_1SDV_ 2020.09.27.	10 m	25.55	0.8	0.93	0.95	92.27
S1B_IW_GRDH_1SDV_ 2021.10.04.	10 m	25.51	1.0	0.9	0.94	91.84

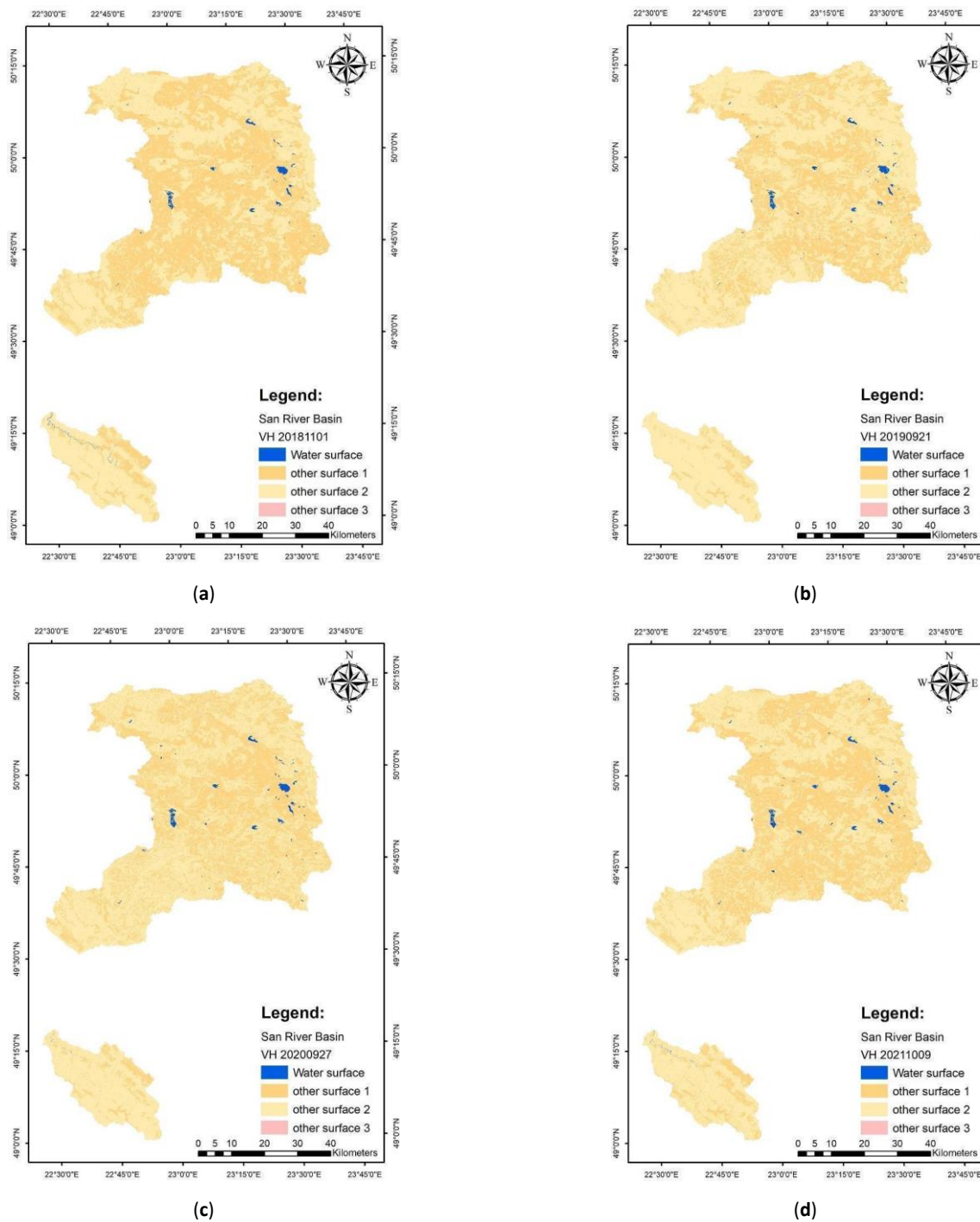


Figure 15. Maps of the San River basin created using Sentinel-1 (SAR) data and using filters (Lee) and MLC classification. Map of classified area types based on VH polarization data for the dry season: (a) November 2018, (b) September 2019, (c) September 2020, and (d) October 2021.

According to the SAR data, in the San River basin, the largest values of water surface area were recorded in 2020 at 25.55 thousand km² and in 2021 at 25.51 thousand km², which are shown in Table 8. This indicates that, according to SAR data, 2020 and 2021 were wetter than 2018 and 2019.

The water surface UA statistic for the San River basin created using Sentinel-1 (SAR) ranged from 0.9 to 1, which indicates the quality of the accuracy determination procedure.

The Kappa coefficient is a measure of the accuracy of image classification [1–6,17,18,28,33,48], and the statistical indicator UA of the water surface determines the quality of the user procedure

for determining the accuracy. All constructed maps with the selection of water surfaces presented in this research have high accuracy indicators of the Kappa coefficient and the UA of the water surface. For the Bug River basin, according to multispectral data (NDWI), Kappa accuracy indicators range from 76.71% to 85.88% and UA indicators range from 0.92 to 1; according to radar data, Kappa coefficients range from 87.61% to 93.43%, and the UA ranges from 0.87 to 1. For the Dniester River basin, according to multispectral data (NDWI), the Kappa accuracy indicators range from 79.76% to 87.25%, while the UA ranges from 0.08 to 1; using radar data, the Kappa coefficient ranges from 91.41% to 97.18% and the UA ranges from 0.94 to 1. For the San River basin, according to multispectral data (NDWI), the Kappa accuracy indicators range from 76.28% to 88.65%, and the UA is 1; according to radar data, the Kappa coefficient ranges from 91.84% to 92.87% and the UA from 0.9 to 1.

For the Bug River basin, 2018 and 2021 were wetter than 2019 and 2020, both according to the optical and radar data. For the Dniester River basin, 2018 was the wettest year, both according to the optical and radar data. However, 2019 was wetter according to the optical data and 2020 according to the radar data. In our research, calculations were applied to the Kappa accuracy coefficient, which has better values for radar data. Therefore, it is better to base observations on the results of the radar data. For the San River basin, the years 2020 and 2021 are wet (according to the radar data).

According to the data from the Climate Change Portal (accessed on 1 June 2022 <https://climate.copernicus.eu/precipitation-relative-humidity-and-soil-moisture>) in the graph (monthly European surface air relative humidity anomalies) for the period from 2018 to 2021 for Europe, 2018 and 2021 are wetter. This is an additional indication of the accuracy of the data obtained in this research for the Bug and Dniester River basins.

The obtained statistical indicators of high accuracy in this research show the excellent results of the applied technique and its prospects for application in future research related to the monitoring of water surfaces according to remote sensing data. In addition, the mapping results can be included in studying the changes in the water resources of the Ukrainian–Polish border, especially the Ukrainian part, which is not included in European databases.

5. Discussion

The application of remote sensing data for the identification and mapping of water bodies has advantages in the frequency of data updates, the direct accessibility of the data (open service portals), the new technologies for processing them, and the wide range of topics covered. But there are difficulties in the processing and using of these data. For example, weather conditions such as a cloud cover are important for optical data, while radar data require a complex processing algorithm, as background noise can mix with water pixels and general difficulties can arise in the inefficient identification of water bodies with mixed pixels.

The developed methodology made it possible to identify, map, and calculate the area of water bodies and wetlands during the low-water seasons from 2018 to 2021 in the Bug, Dniester, and San River basins. In addition, the results were compared with optical and radar data. But the described methodology, similar to other methods, has its advantages and disadvantages. For example, the optical data used (RGB composite) have a wide spectral band, which allows for identifying not only open water surfaces but also wetlands. With frequent monitoring, it is possible to detect the dryness/wetness trend in the study area. However, to use optical data, a weather filter is a necessary condition; that is, images must have 0% cloud cover. For radar data, there is no such problem, but the processing involves a more complex algorithm with calibration, terrain correction, the application of filters to remove thermal noise, and special filters for water bodies. In addition, radar images clearly identify the water surface and, in the case of wetlands, the best results are obtained using multispectral data. The methodology used, in addition to processing satellite images, includes a mapping stage with classification and post-classification processing, which directly affects the quality of the results obtained.

A total of 44 satellite images were processed in this study. The monitoring was conducted from 2018 to 2021 in the driest month of the year (in autumn). For the NDWI, 24 images were used. For the RGB composite (band: 11, 8, 2), 8 images were used, and for the identification of the water surface according to SAR and VH polarization (Sentinel-1), 12 images were used. The coverage of all three basins of the Bug, Dniester, and San rivers consists of eight Sentinel-2 images or three Sentinel-1 images.

The main advantages of the developed methodology are a combination of options for focusing and improving image quality and, accordingly, ensuring the accurate identification of water surfaces and wetlands. By applying multiple filters (including the Lee filter) to the radar data, we were able to remove noise and account for relief, as was also performed by other researchers [2–4,6,17]. Using MLC classification [16,26] with post-classification processing (a complex of options), a significant improvement in image quality was achieved. All of the methodological options combined made it possible to obtain the optimal result for mapping water bodies and wetlands, taking into account all characteristics of the study area.

The results were evaluated numerically and graphically using statistical indicators: Kappa coefficients, overall accuracy (OA), user accuracy (UA), and producer accuracy (PA). To check the accuracy of the results obtained for the radar and optical data, the Kappa coefficient was calculated for the test area (within the study area) and for all river basin maps. The Kappa coefficient was obtained in the test area for multispectral data for RGB (range: 11, 8, 2) (84.95%), for the NDWI (85.88%), and for radar data (88.84%). The values of the obtained accuracy indicators indicate the prospects of applying the developed methodology for identifying water bodies in the study area. Furthermore, using the described methodology, maps with water surfaces for the period of the driest month of the year from 2018 to 2021 were constructed to review the dynamics of changes and to verify the accuracy of the results. The Kappa coefficient of the accuracy for the Bug River basin area for optical data in different periods ranged from 76.71% to 85.88% and, for radar data, it ranged from 87.61% to 93.43%. For the Dniester River basin area, it ranged from 79.76% to 87.25% based on optical data and from 91.41% to 97.18% based on radar data, and for the San River basin area, it ranged from 76.28% to 88.65% based on optical data and from 91.84% to 92.87% based on radar data. When assessing accuracy, the highest values were achieved for overall accuracy (OA), with maximum values of 0.95 (for SAR) and 0.91 (for optical data). The highest values were in user accuracy (UA), with a maximum value of 1 for both SAR and optical data.

The accuracy values obtained from radar data in all river basins are higher than those from optical data, which indicates a greater accuracy in identifying water surfaces, specifically from SAR data; however, the wide spectral range of optical data allowed us to map not only open water surfaces, but also wetlands, which may be seasonal with vegetation or small areas and are not recorded on radar.

High statistical indicators of the accuracy of the method show the excellent results of the presented method, as well as its prospects for application in future research related to the monitoring of water surfaces according to remote sensing data. In future studies, this methodology can be applied to data from other satellites with the same spectral bands in order to monitor changes in water surfaces in a frequent time range, for example, to track seasonal or annual changes in different study areas. The developed technique can be recommended for the identification and mapping of water bodies and wetlands and for monitoring flooded areas at a large scale of 1:500,000 and a small scale of 1:1000 as the image resolution of 10 m allows for it. The obtained results for the basins of the Bug, Dniester, and San rivers using both optical and radar data can be used for the accurate monitoring of changes in the water surface and wetlands.

6. Conclusions

In this research, based on the experience of contemporary researchers, a methodology was developed to identify water surfaces and wetlands using Sentinel-2B optical data and

Sentinel-1A/B SAR data, taking into account the peculiarities of the study areas of the Bug, Dniester, and San River basins. Based on the optical data, we decided to apply the classic NDWI index and RGB composition with MLC classification and post-classification processing in ArcGis 10.6.1., which included the use of filters, pixel generation, boundary smoothing, and small area removal. The process of identifying water surfaces using Sentinel-1 radar data with VH polarization included a complex processing algorithm in the SNAP program namely involving calibration, the alignment and correction of relief, the application of filters to remove thermal noise, and the application of the Lee filter, which is used specifically for water bodies.

For the first time, using the developed method, water surfaces and wetlands within the basins of the Bug, Dniester, and San rivers, which are located along the Polish–Ukrainian border, were identified and mapped according to the remote sensing data. The obtained mapping results can be included in future research on changes in water resources in this area, especially the Ukrainian part, which is not included in European databases.

The results were evaluated numerically and graphically using statistical indicators: Kappa coefficients, overall accuracy (OA), user accuracy (UA), and producer accuracy (PA). This methodology was employed to identify the years with higher humidity. For the Bug River basin, it was 2018 and 2021; for the Dniester River basin, it was 2018 and 2020; and for the San River basin, it was 2020 and 2021. The obtained high statistical accuracy indicators in this research testify to the effective results of the presented method and the prospects for its application in future research into monitoring changes in water resources. This would help to update data on changes in the water surface area and determine drought/wetness trends over a season, year, or several years. In addition, the developed methodology can be recommended for the identification of water bodies (according to radar data) and wetlands (according to optical data) in various study areas, including areas larger than 1000 km² with contrasting reliefs.

Author Contributions: Methodology, T.M.; Validation, T.M.; Writing—original draft, T.M.; Project administration, T.S. All authors have read and agreed to the published version of the manuscript.

Funding: The research was carried out within the following projects: (1) No. 2018-1-0137 “EU-waterrres: EU-integrated management system of cross-border groundwater resources and anthropogenic hazards”, which benefits from a EUR 2.447.761 grant Iceland, Liechtenstein, and Norway through the EEA and Norway Grants Fund for Regional Cooperation; (2) the program of the Minister of Science and Higher Education entitled “PMW” in the years 2020–2023, agreement No. W82/RF-COOPERATION/2020.

Data Availability Statement: The research was done as part of Project “EU-waterrres: EU-integrated management system of cross-border groundwater resources and anthropogenic hazards”. <https://eu-waterrres.eu/web-app/>.

Conflicts of Interest: The authors declare no conflict of interest.

References

1. Marzi, D.; Gamba, P. Inland water body mapping using multitemporal Sentinel-1 SAR data. *IEEE J. Sel. Top. Appl. Earth Obs. Remote Sens.* **2021**, *14*, 11789–11799. [\[CrossRef\]](#)
2. Jiang, H.; Wang, M.; Hu, H.; Xu, J. Evaluating the performance of Sentinel-1A and Sentinel-2 in small waterbody mapping over urban and mountainous regions. *Water* **2021**, *13*, 945–960. [\[CrossRef\]](#)
3. Ksėnak, L’.; Pukanská, K.; Bartoš, K.; Blišťan, P. Assessment of the usability of SAR and optical satellite data for monitoring spatio-temporal changes in surface water: Bodrog river case study. *Water* **2022**, *14*, 299. [\[CrossRef\]](#)
4. Shen, G.; Fu, W.; Guo, H.; Liao, J. Water body mapping using long time series Sentinel-1 SAR data in Poyang Lake. *Water* **2022**, *14*, 1902. [\[CrossRef\]](#)
5. Tian, H.; Li, W.; Wu, M.; Huang, N.; Li, G.; Li, X.; Niu, Z. Dynamic monitoring of the largest Freshwater Lake in China using a new water index derived from high spatiotemporal resolution Sentinel-1A data. *Remote Sens.* **2017**, *9*, 521–528. [\[CrossRef\]](#)
6. Kumar, D. Urban objects detection from C-band synthetic aperture radar (SAR) satellite images through simulating filter properties. *Sci. Rep.* **2021**, *11*, 1–24. [\[CrossRef\]](#) [\[PubMed\]](#)

7. Abdikan, S.; Sanli, F.B.; Ustuner, M.; Calò, F. Land cover mapping using Sentinel-1 SAR data. In Proceedings of the International Archives of the Photogrammetry, Remote Sensing and Spatial Information Sciences, XXIII ISPRS Congress, Prague, Czech Republic, 12–19 July 2016. [\[CrossRef\]](#)
8. Yesou, H.; Pottier, E.; Mercier, G.; Grizonnet, M.; Haouet, S.; Giros, A.; Faivre, R.; Huber, C.; Michel, J. Synergy of Sentinel-1 and Sentinel-2 imagery for wetland monitoring information extraction from continuous flow of sentinel images applied to water bodies and vegetation mapping and monitoring. In Proceedings of the Conference: IGARSS 2016—IEEE International Geoscience and Remote Sensing, Beijing, China, 10–15 July 2016. [\[CrossRef\]](#)
9. Luca, G.D.; Silva, J.M.N.; Fazio, S.D.; Modica, G. Integrated use of Sentinel-1 and Sentinel-2 data and open-source machine learning algorithms for land cover mapping in a Mediterranean region. *Eur. J. Remote Sens.* **2022**, *55*, 52–70. [\[CrossRef\]](#)
10. Souza, W.d.O.; Reis, L.G.d.M.; Ruiz-Armenteros, A.M.; Velede, D.; Ribeiro Neto, A.; Fragoso, C.R., Jr.; Cabral, J.J.d.S.P.; Montenegro, S.M.G.L. Analysis of environmental and atmospheric influences in the use of SAR and optical imagery from Sentinel-1, Landsat-8, and Sentinel-2 in the operational monitoring of reservoir water level. *Remote Sens.* **2022**, *14*, 2218–2245. [\[CrossRef\]](#)
11. Jiakun, T.; Shaoxia, X.; Yu, L.; Xiubo, Y.; Houlang, D.; Han, X.; Chuanpeng, Z. Assessing habitat suitability for wintering geese by using Normalized Difference Water Index (NDWI) in a large floodplain wetland, China. *Ecol. Indic.* **2021**, *122*, 107260–107268. [\[CrossRef\]](#)
12. Pal, S.; Sarda, R. Measuring the degree of hydrological variability of riparian wetland using hydrological attributes integration (HAI) histogram comparison approach (HCA) and range of variability approach (RVA). *Ecol. Indic.* **2021**, *120*, 106966–106979. [\[CrossRef\]](#)
13. Khatun, R.; Talukdar, S.; Pal, S.; Kundu, S. Measuring dam induced alteration in water richness and eco-hydrological deficit in flood plain wetland. *J. Environ. Manag.* **2021**, *285*, 112157–112172. [\[CrossRef\]](#)
14. Kwang, C.; Osei Jnr, M.E.; Sarpong, A.A. Comparing of Landsat 8 and Sentinel 2A using Water Extraction Indexes over Volta River. *JGG* **2018**, *10*, 1–7. [\[CrossRef\]](#)
15. Harapenta Surbakti, A.F.; Oktarina, M.; Putri Firdaus, T.; Ibrahim, M.M. Preliminary investigation of geothermal potential with remote sensing based on satellite imagery: Case study in Air Putih area, Lebong regency, Bengkulu. In Proceedings of the 10th ITB International Geothermal Workshop, Bandung Institute of Technology, Kota Bandung, Indonesia, 26–29 July 2021.
16. Sekertekin, A. A Survey on global thresholding methods for mapping open water body using Sentinel-2 satellite imagery and Normalized Difference Water Index. *Arch. Comput. Method Eng.* **2019**, *13*, 1335–1347. [\[CrossRef\]](#)
17. Jiang, W.; Ni, Y.; Pang, Z.; Li, X.; Ju, H.; He, G.; Lv, J.; Yang, K.; Fu, J.; Qin, X. An effective water body extraction method with new water index for Sentinel-2 imagery. *Water* **2021**, *13*, 1647. [\[CrossRef\]](#)
18. Du, Y.; Zhang, Y.; Ling, F.; Wang, Q.; Li, W.; Li, X. Water bodies' mapping from Sentinel-2 imagery with Modified Normalized Difference Water Index at 10-m spatial resolution produced by sharpening the SWIR Band. *Remote Sens.* **2016**, *8*, 354–372. [\[CrossRef\]](#)
19. Kati, I.E.; Nakhcha, C.; Bakhchouch, O.E.; Tabyaoui, H. Application of Aster and Sentinel-2A images for geological mapping in Arid Regions: The Safsafate area in the Neogen Guercif basin, Northern Morocco. *IJARSG* **2018**, *7*, 2782–2792. [\[CrossRef\]](#)
20. Yang, X.; Zhao, S.; Qin, X.; Zhao, N.; Liang, L. Mapping of urban surface water bodies from Sentinel-2 MSI imagery at 10 m resolution via NDWI-based image sharpening. *Remote Sens.* **2017**, *9*, 596–614. [\[CrossRef\]](#)
21. Enea, A.; Urzica, A.; Breaban, I.G. Remote sensing, GIS and HEC-RAS techniques, applied for flood extent validation, based on Landsat imagery, Lidar and hydrological data. Case study: Baseu River, Romania. *J. Environ. Prot. Ecol.* **2018**, *19*, 1091–1101.
22. Vera-Herrera, L.; Soria, J.; Pérez, J.; Romo, S. Long-term hydrological regime monitoring of a mediterranean agro-ecological wetland using Landsat imagery: Correlation with the water renewal rate of a Shallow Lake. *J. Hydrol.* **2021**, *172*, 1–21. [\[CrossRef\]](#)
23. Das, S. Characterization of surface geological material in Northwest India and adjoining areas of Pakistan using Normalized Difference Water Index, land surface temperature and silica index. *J. Indian Soc. Remote Sens.* **2018**, *46*, 1645–1656. [\[CrossRef\]](#)
24. Ji, L.; Zhang, L.; Wylie, B. Analysis of dynamic thresholds for the Normalized Difference Water Index. *Photogramm. Eng. Remote Sens.* **2009**, *75*, 1307–1317. [\[CrossRef\]](#)
25. Ali, M.I.; Dirawan, G.D.; Hasim, A.H.; Abidin, M.R. Detection of changes in surface water bodies urban area with NDWI and MNDWI methods. *Int. J. Adv. Sci. Eng. Inf. Technol.* **2019**, *9*, 946–951. [\[CrossRef\]](#)
26. Feyisa, G.L.; Meilby, H.; Fensholt, R.; Proud, S.R. Automated Water Extraction Index: A new technique for surface water mapping using Landsat imagery. *Remote Sens. Environ.* **2014**, *140*, 23–35. [\[CrossRef\]](#)
27. Rokni, K.; Ahmad, A.; Selamat, A.; Hazini, S. Water feature extraction and change detection using multitemporal landsat imagery. *Remote Sens.* **2014**, *6*, 4173–4189. [\[CrossRef\]](#)
28. Ko, B.C.; Kim, H.H.; Nam, J.Y. Classification of potential water bodies using landsat 8 OLI and a combination of two boosted random forest classifiers. *Sensors* **2015**, *15*, 13763–13777. [\[CrossRef\]](#) [\[PubMed\]](#)
29. Dash, P.; Sar, J. Identification and validation of potential flood hazard area using GIS-based multi-criteria analysis and satellite data-derived water index. *J. Flood Risk Manag.* **2020**, *13*, 1–14. [\[CrossRef\]](#)
30. Reshitnyk, L.; Costa, M.; Robinson, C.; Dearden, P. Evaluation of WorldView-2 and acoustic remote sensing for mapping benthic habitats in temperate coastal Pacific waters. *Remote Sens.* **2014**, *153*, 7–23. [\[CrossRef\]](#)
31. Sunder, S.; Ramsankaran, R.; Ramakrishnan, B. Inter-comparison of remote sensing sensing-based shoreline mapping techniques at different coastal stretches of India. *Environ. Monit. Assess.* **2017**, *189*, 290–302. [\[CrossRef\]](#) [\[PubMed\]](#)

32. Mustafa, M.T.; Hassoon, K.I.; Hussain, H.M.; Modher, H. Using water indices (NDWI, MNDWI, NDMI, WRI AND AWEI) to detect physical and chemical parameters by apply remote sensing and Gis techniques. *Int. J. Res. Granthaalayah* **2017**, *5*, 117–128. [\[CrossRef\]](#)
33. Lai, X.; Shankman, D.; Huber, C.; Yesou, H.; Huang, Q.; Jiang, J. Sand mining and increasing Poyang Lake's discharge ability: A reassessment of causes for lake decline in China. *J. Hydrol.* **2014**, *519*, 1698–1706. [\[CrossRef\]](#)
34. Tran, H.; Nguyen, P.; Ombadi, M.; Hsu, K.; Sorooshian, S.; Andreadis, K. Improving hydrologic modeling using cloud-free MODIS flood maps. *J. Hydrometeorol.* **2019**, *20*, 2203–2214. [\[CrossRef\]](#)
35. Hancock, S.; Baxter, R.; Evans, J.; Huntley, B. Evaluating global snow water equivalent products for testing land surface models. *Remote Sens.* **2013**, *128*, 107–117. [\[CrossRef\]](#)
36. Lee, H.; Yuan, T.; Jung, H.C.; Beighley, E. Mapping wetland water depths over the central Congo Basin using PALSAR ScanSAR, Envisat altimetry, and MODIS VCF data. *Remote Sens.* **2015**, *159*, 70–79. [\[CrossRef\]](#)
37. Feng, L.; Hu, C.; Chen, X.; Cai, X.; Tian, L.; Gan, W. Assessment of inundation changes of Poyang Lake using MODIS observations between 2000 and 2010. *Remote Sens.* **2012**, *121*, 80–92. [\[CrossRef\]](#)
38. Wu, G.; Liu, Y. Capturing variations in inundation with satellite remote sensing in a morphologically complex, large lake. *J. Hydrol.* **2015**, *523*, 14–23. [\[CrossRef\]](#)
39. Feng, L.; Hub, C.; Chen, X.; Song, Q. Influence of the Three Gorges Dam on total suspended matters in the Yangtze Estuary and its adjacent coastal waters: Observations from MODIS. *Remote Sens.* **2014**, *140*, 779–788. [\[CrossRef\]](#)
40. Melnichenko, T. Remote research of geotectonic processes using the satellites MODIS (Aqua/Terra) images in the GIS program (for example, the Black Sea). In Proceedings of the 17th International Conference on Geoinformatics—Theoretical and Applied Aspects, EAGE, Kiev, Ukraine, 14–17 May 2018. [\[CrossRef\]](#)
41. Melnichenko, T. Estimation of activity the methane seepage from the Black Sea floor using MODIS images and geosciences data. *J. Geol. Geogr. Geoecology* **2018**, *26*, 135–142. [\[CrossRef\]](#)
42. Hou, X.; Feng, L.; Duan, H.; Chen, X.; Sunc, D.; Shi, K. Fifteen-year monitoring of the turbidity dynamics in large lakes and reservoirs in the middle and lower basin of the Yangtze River, China. *Remote Sens.* **2017**, *190*, 107–121. [\[CrossRef\]](#)
43. Gu, Y.; Brown, J.F.; Verdin, J.P.; Wardlow, B. A five-year analysis of MODIS NDVI and NDWI for grassland drought assessment over the central Great Plains of the United States. *Geophys. Res. Lett.* **2007**, *34*, 407–412. [\[CrossRef\]](#)
44. Chen, F.; Chen, X.; Van de Voorde, T.; Roberts, D.; Jiang, H.; Xu, W. Open water detection in urban environments using high spatial resolution remote sensing imagery. *Remote Sens.* **2020**, *242*, 111706–111722. [\[CrossRef\]](#)
45. Rahman, M.R.; Thakur, P.K. Detecting, mapping and analysing of flood water propagation using synthetic aperture radar (SAR) satellite data and GIS: A case study from the Kendrapara District of Orissa State of India. *Egypt. J. Remote Sens. Space Sci.* **2018**, *21*, 37–41. [\[CrossRef\]](#)
46. Chapman, B.; McDonald, K.; Shimada, M.; Rosenqvist, A.; Schroeder, R.; Hess, L. Mapping regional inundation with spaceborne L-Band SAR. *Remote Sens.* **2015**, *7*, 5440–5470. [\[CrossRef\]](#)
47. Bolanos, S.; Stiff, D.; Brisco, B.; Pietroniro, A. Operational surface water detection and monitoring using Radarsat 2. *Remote Sens.* **2016**, *8*, 285–302. [\[CrossRef\]](#)
48. Evans, T.L.; Costa, M. Landcover classification of the Lower Nhecolândia subregion of the Brazilian Pantanal Wetlands using ALOS/PALSAR, RADARSAT-2 and ENVISAT/ASAR imagery. *Remote Sens.* **2013**, *128*, 118–137. [\[CrossRef\]](#)
49. Scott, K.A.; Buehner, M.; Caya, A.; Carrieres, T. A preliminary evaluation of the impact of assimilating AVHRR data on sea iceconcentration analyses. *Remote Sens.* **2013**, *128*, 212–223. [\[CrossRef\]](#)
50. Szombara, S.; Lewińska, P.; Zadło, A.; Róg, M.; Maciuk, K. Analyses of the pradnik riverbed shape based on archival and contemporary data sets—Old maps, LiDAR, DTMs, orthophotomaps and cross-sectional profile measurements. *Remote Sens.* **2020**, *12*, 2208–2237. [\[CrossRef\]](#)
51. Dronova, I.; Gong, P.; Wang, L.; Zhong, L. Mapping dynamic cover types in a large seasonally floodedwetland using extended principal component analysis and object-based classification. *Remote Sens.* **2015**, *158*, 193–206. [\[CrossRef\]](#)
52. Wilusz, D.C.; Zaitchik, B.F.; Anderson, M.C.; Hain, C.R.; Yilmaz, M.T.; Mladenova, I.E. Monthly flooded area classification using low resolution SAR imagery in the Sudd wetland from 2007 to 2011. *Remote Sens.* **2017**, *194*, 205–218. [\[CrossRef\]](#)
53. Gao, B.-C. NDWI—A normalized difference water index for remote sensing of vegetation liquid water from space. *Remote Sens. Environ.* **1996**, *58*, 257–266. [\[CrossRef\]](#)
54. Solovey, T.; Janica, R.; Przygodzka, M.; Harasymchuk, V.; Medvid, H. Geological and hydrogeological conditions of the PL-UA borderland. In *Assessment of the Resources of Transboundary Groundwater Reservoirs for the 2 Pilot Areas*; Solovey, T., Harasymchuk, V., Eds.; PGI-NRI: Warsaw, Poland, 2021; pp. 28–36. (In Polish) [\[CrossRef\]](#)
55. Solovey, T.; Janica, R.; Harasymchuk, V.; Przychodzka, M.; Medvid, H.; Yanush, L. Transboundary groundwater flows between Poland and Ukraine: The role of join assessments and international frameworks on water resources management. *Ecohydrol. Hydrobiol.* **2022**, *in print*.

Disclaimer/Publisher's Note: The statements, opinions and data contained in all publications are solely those of the individual author(s) and contributor(s) and not of MDPI and/or the editor(s). MDPI and/or the editor(s) disclaim responsibility for any injury to people or property resulting from any ideas, methods, instructions or products referred to in the content.